

Seismic Risk for Existing Buildings

Development of fragility curves using dynamic analysis. Trial applications for masonry and RC buildings in Switzerland

December 2014

EPFL-ENAC-IIC-IMAC

Commissioned by the Federal Office for the Environment (FOEN)

Impressum

- Commissioned by** Federal Office for the Environment (FOEN)
Earthquake Mitigation Section
CH-3003 Bern
The FOEN is an agency of the Federal Department of the Environment, Transport, Energy and Communications (DETEC)
- Contractor** APPLIED COMPUTING AND MECHANICS LABORATORY
EPFL-ENAC-IIC-IMAC
Station 18, CH-1015 Lausanne
Switzerland
- Authors** Dr. A. Karbassi and Dr. P. Lestuzzi
- Citation** Karbassi, A., and Lestuzzi P. (2014) Seismic risk for existing buildings in Switzerland – development of fragility curves for masonry buildings, Ecole Polytechnique Fédérale de Lausanne, Lausanne, Switzerland, report prepared under contract to the Federal Office for the Environment (FOEN), 56 p.
- FOEN support** B. Duvernay, Dr. N. Jamali, E. Kölz, and Dr. C. Michel
- Note** This study/report was prepared under contract to the Federal Office for the Environment (FOEN). The contractor bears sole responsibility for the content.

Summary

Common part

Seismic examination of existing buildings in Switzerland is currently performed using the pre-standard SIA 2018 (2004) of the Swiss society of engineers and architects (SIA). In the seismic examination of existing buildings according to SIA 2018, a minimal acceptable safety level as well as the commensurability of retrofitting measures must be verified. The key element to do these verifications is the relationship between the degree of compliance of an existing building with the seismic safety requirements for new buildings and the risk to people inside the building. In SIA 2018, this relationship is presented as a curve with the so-called compliance factor of the building in abscissa and the annual casualty probability for people inside the building in ordinate. This curve was established based on risk calculations using empirical methods as well as on expert judgment to link empirical building vulnerability classes with plausible ranges of the compliance factor [Kölz et al., 2006].

In 2015 the pre-standard SIA 2018 will be replaced by the new building code SIA 269/8 "Existing structures – Earthquake". In this new building code the central concepts of minimal safety level and commensurability of measures of SIA 2018 will be kept and adapted to the current state of knowledge. For this, the curve linking the compliance factor with the risk to people in SIA 2018 must be verified. Furthermore, in order to extend the commensurability criterion to cope with damage to property, it is intended to propose a new curve linking the compliance factor with property damage.

As a support to the issuance of the new building code SIA 269/8 and in the interest of providing better tools for the probabilistic seismic risk computation for existing buildings in Switzerland, the Federal Office for the Environment (FOEN) initiated a research project in 2010 with the following objectives:

- Provide a consistent set of probabilistic hazard data in EMS-Intensity and spectral acceleration values for 3 to 5 sites covering the range of seismic hazard in Switzerland
- Develop vulnerability functions for representative Swiss buildings, including uncertainties
- Prepare a reusable documented computational framework for the probabilistic risk quantification
- Quantify the dispersion of risk according to different available methodologies and relevant uncertainties
- Obtain verification data for the risk curve for people in the pre-standard SIA 2018 and data for the risk curve for property in the new building SIA 269/8.

The partners of this project which was conducted by FOEN were the Swiss Seismological Service (SED), the Swiss Institute of Technology / applied computing and mechanics laboratory (IMAC) and Risk&Safety AG (R&S):

- SED provided the hazard data for the three locations Zurich, Basel, and Sion (two sites) as well as amplification factors considering local site effects. Hazard data was provided in 2 formats as a function of spectral acceleration and EMS-Intensity including percentile curves, which were demonstrating uncertainties of data.
- IMAC has provided fragility curves for 5 benchmark buildings through nonlinear dynamic analysis. For two benchmark buildings fragility curves after retrofitting have also been provided. IMAC also computed the compliance factors for all the benchmarks using standard engineering procedures.
- R&S developed and documented a model to calculate risk combining the probabilistic hazard data and the fragility curves for both the mechanical and empirical approaches. The risk was then calculated for all the benchmark buildings.

Specific part for IMAC report

This report concerns the investigations performed by the Applied Computing and Mechanics Laboratory (IMAC) of EPFL. It mainly contains the calculations to develop fragility curves for benchmark buildings using nonlinear dynamic analyses. The related compliance factors for the benchmark building are also determined.

Seven benchmark buildings (5 originals + 2 retrofitted), four unreinforced masonry (URM), two dual system (masonry and reinforced concrete), and one reinforced concrete (RC) buildings which are representative of the main classes of typical URM and RC buildings with stiff and semi-rigid floors in Switzerland are first selected. These buildings are modelled using expected values instead of design or characteristic values for mechanical material properties in order to simulate as close as possible their real seismic behaviour. Nonlinear dynamic analyses are then performed using the Applied Element Method (AEM). This method, which is based on dividing structural members into virtual elements connected through springs (no common nodes unlike Finite Element Method) can simulate large displacements and elements progressive separation through successive failure of those springs. The AEM numerical modelling has the ability to simulate in-plane and out-of-plane failure modes in masonry units and in masonry structures due to static and dynamic loadings.

A clear definition of the damage grades is crucial to conduct the seismic vulnerability evaluation. The EMS-98 damage grades are essentially used in this study to determine the limit states from the nonlinear dynamic analysis. Regarding seismic loading, 50 ground motions are used. The ground motion records are chosen from the European ground motion record database with a condition of selecting those records which have spectral acceleration values covering the range of the spectral acceleration values provided by the Swiss Seismological Service for different cities in Switzerland.

The fragility curve for a building presents the probability of reaching and/or exceeding a damage grade, given an engineering demand parameter (e.g., peak ground acceleration, spectral acceleration). The fragility curves developed in this study are presented in the form of a two-parameter lognormal distribution function. The only uncertainty considered in the development of the fragility curves is the uncertainty related to the record-to-record variability. Such an uncertainty is taken into account by applying the 50 ground motion records in the dynamic analysis. It should be noted that after several trials and discussions inside the project team, it was finally decided to use the spectral acceleration values related to the average period of each building corresponding to damage grade 2 as a reference hazard parameter to develop the fragility curves. Comparison with fragility curves from other methods shows similar trends but generally less pessimistic, due to the use of expected values for mechanical material properties.

Furthermore compliance factors according to pre-standard SIA 2018 are computed for the benchmark buildings. Displacement-based analysis and force-based analysis are both used to determine the values of the compliance factors. These engineering analyses are performed according to the usual procedure proposed in the Swiss building codes and without refined modelling.

Table of contents

1. Objectives	1
2. Selection of prototype buildings	2
2.1. Studied buildings	2
2.2. Material properties	3
3. Methodology	6
3.1. Progressive collapse in masonry structures	6
3.2. Application of the AEM for masonry and reinforced concrete	7
3.3. Verification of AEM with experimental tests	9
3.3.1 In-plane loading	9
3.3.2 Out-of-plane loading	9
3.3.3 Half-scale 4 storey RC-URM building	11
3.4. Definition of damage grades in masonry buildings and RC buildings	13
3.5. Selection of ground motion records	15
3.6. Numerical model for the studied buildings	16
3.7. Development of fragility curves	18
4. Results of dynamic analyses	19
4.1. Identifications of damage grades	19
4.2. Progressive change of modal period with damage	22
4.3. Results for the building CHB30	23
4.4. Results for the building CHB30 ORG	24
4.5. Results for the building YVR14	25
4.6. Results for the building SECH7	26
4.7. Results for the building STD40 ORG	27
4.8. Results for the building STD40	28
4.9. Results for the building SUVA	29
4.10. Fragility curves of the benchmark buildings	30
4.10.1. Fragility curves for CHB30	30
4.10.2. Fragility curves for CHB30 ORG	31
4.10.3. Fragility curves for YVR14	32
4.10.4. Fragility curves for SECH7	32
4.10.5. Fragility curves for STD40 ORG	33
4.10.6. Fragility curves for STD40	34
4.10.7. Fragility curves for SUVA	34
5. Discussion of the results	36
5.1. Compliance factor of the studied buildings	36
5.2. Comparing with results from other methods	41
5.3. Standard error in the estimation of the engineering demand parameters	44
6. Conclusion	45
References	46
Appendix A. Ground motion records	49
Appendix B. Information summary for the benchmark buildings	50

1. Objectives

The Swiss Federal Office for the Environment (FOEN) has initiated the project “*Seismic Risk for Existing Building*” (hereafter called FOEN project) with the following objectives.

- 1) Provide a consistent set of probabilistic hazard data in EMS-Intensity and spectral acceleration values for 3 to 5 sites covering the range of seismic hazard levels in Switzerland
- 2) Develop vulnerability functions for representative Swiss buildings, including uncertainties
- 3) Prepare a reusable documented computational framework for the risk quantification
- 4) Calculate a quantified dispersion of risk assessment according to different available methodologies and relevant uncertainties
- 5) Obtain verification data for the risk curves in the pre-standard SIA 2018.

The goal of the FOEN project is to compare the seismic risk quantification for typical Swiss buildings using both EMS-based methodologies (empirical approaches) on one hand, and more modern vulnerability functions derived from displacement-based analyses (mechanical approach), on the other hand. The main focus of this report is to present the methodology performed by IMAC to develop fragility curves for four unreinforced masonry (URM), two dual system (masonry and reinforced concrete), and one reinforced concrete (RC) buildings. The URM and RC buildings studied here are representative for residential masonry buildings with stiff and semi-rigid floors, in Switzerland. In the context of seismic vulnerability evaluation of existing buildings, only dynamic-based methods are capable to take into account the dynamic behaviour in the numerical models. The proposed methodology uses an Applied Element-based approach to overcome the limitations of a FE-based method which is not able to simulate the progressive collapse case for masonry buildings.

2. Selection of prototype buildings

2.1. Studied buildings

For this study, four unreinforced masonry (URM), two dual system (masonry and reinforced concrete), and one reinforced concrete (RC) buildings which are representative for the main classes of typical URM and RC buildings with stiff and semi-rigid floors in Switzerland are selected and described in the following sections.

2.1.1. Stone masonry building with RC slabs (*Chablais 30 after retrofit, abbreviated hereafter CHB30*)

The first structure is a stone masonry building with concrete slabs (Figure 1.a) located in Lausanne. It is a 14m by 12m (in plan) rubble stone masonry with a total number of 6 storeys. The building has 14 walls in the longitudinal direction and 15 walls in the transversal direction. The width of the walls varies between 25 cm to 60 cm, and its average storey height is 3 meters. The thickness of the reinforced concrete slab for this project is assumed to be 20 cm.

2.1.2. Stone masonry building with timber slab (*Chablais 30 before retrofit, abbreviated hereafter CHB30 ORG*)

This building is the same as CHB30, but with timber slabs which represents the original condition of the building before retrofitting took place.

2.1.3. Brick masonry building (*Léon Jaquier 14-16, abbreviated hereafter YVR14*)

The second building is a brick masonry structure with RC slabs (Figure 1.b). This 4-storey building is located in Yverdon-Les-Bains. The building is 30 m. by 12 m. (in plan) and it has 37 walls in the longitudinal direction and 16 walls in the transversal direction. The storey height is 2.7 m. The concrete slabs have a thickness of 20 cm.

2.1.4. Brick masonry building (*Secheron 7, abbreviated hereafter SECH7*)

The building is a 7-story brick masonry structure in Geneva with RC slabs (thickness of 18 cm) built in the 60's, as shown in Figure 1.c. The building is 21 m long and 11 m wide with a story height of 2.8 m. The building has several masonry walls in its transvers direction; however, there are very few walls in the longitudinal direction of the building.

2.1.5. Dual system building: brick masonry/RC (*Stand 40, abbreviated hereafter STD40 ORG*)

The building is a 6-story structure located in Geneva with several masonry walls, two RC shear walls (one of which is very short) and several concrete columns, and RC slabs (Figure 1.d). The external concrete and masonry walls start from the second floor. This makes the building to have a soft first storey. The building is about 20 m long, 14 m wide and 25 m high.

2.1.6. Retrofitted dual system building: brick masonry/RC (*Stand 40, abbreviated hereafter STD40*)

This building is the same as STD40 ORG with the external reinforced concrete and masonry walls extended to the first floor to eliminate the soft storey.

2.1.7. Reinforced concrete building (*Léopold-Robert 23*, abbreviated hereafter *SUVA*)

This is an 11-story RC structure with RC slabs in La Chaux-de-Fonds in Switzerland built in 1967 (Figure 1.e). The building is 33 m long and 15 m wide with a story height of 3 m (4m for the first two floors). The first and the fifth floors are considerably softer than their immediate upper floor.

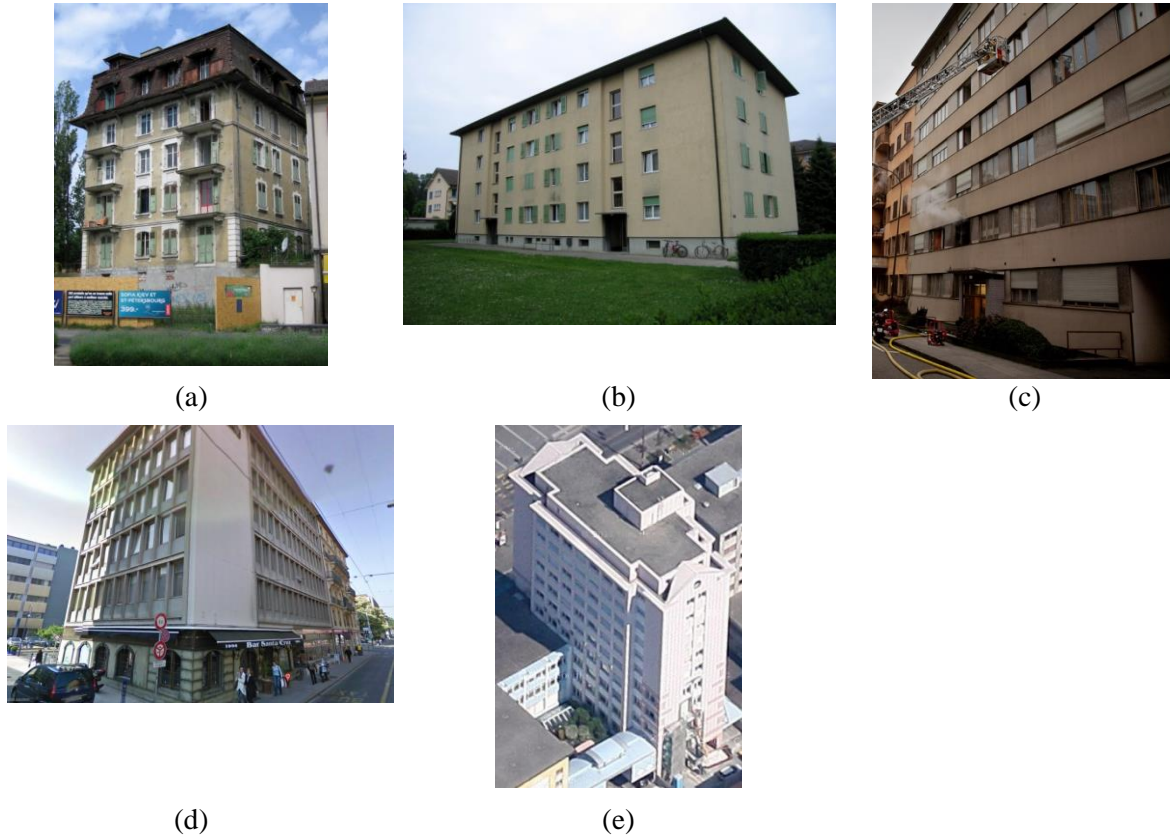


Figure 1: Selected studied buildings in this report
(a) CHB30 (b) YVR14 (c) SECH7 (d) STD40 ORG, and (e) SUVA

Table 1 summarizes the properties for all the studied building shown in Figure 1.

Table 1: Structural characteristics of the studied buildings

	CHB30	CHB30 ORG	YVR14	SECH7	STD40 ORG	STD40	SUVA
Number of stories	6	6	4	7	6	6	11
Year of construction	End of 19 th cent. retrofit in 2009	End of 19 th century	1955	1960's	1956	NA (fictive retrofit)	1967
Structural system	Stone masonry	Stone masonry	Brick masonry	Brick masonry	Dual system (URM+RC)	Dual system (URM+RC)	RC
Floor material	RC	Wood	RC	RC	RC	RC	RC

2.2. Material properties

Table 2 gives the masonry unit, concrete, and steel design properties from different references.

Table 2: Material design properties

Masonry	
E_m modulus of elasticity	1000 f_{xd} (SIA266 2003; EC-6 2005)
f_{xd} compression strength (MPa)	2-5.5 (SIA266 2003; SIA2018 2004)
f_{yd} compression strength (MPa)	$0.3 f_{xd} - 0.5 f_{xd}$ (SIA266 2003)
f_{td} tensile strength (kPa)	150-350 (Lourenco 1998)
Concrete	
E_c modulus of elasticity (GPa)	22 (SIA 262, 2003; Balendran, 1995)
f'_c compression strength (MPa)	33 (SIA262, 2003)
f_t tensile strength (MPa)	3 (SIA262, 2003)
Steel	
E_s modulus of elasticity (GPa)	210 (SIA 262, 2003)
f_y tensile yield stress (MPa)	360 (SIA 2018, 2004; Anand et al., 2007)
f_u ultimate strength (MPa)	500 (SIA 2018, 2004; Kappos et al., 1999)
ϵ_s ultimate strain	0.05 (SIA 262, 2003)

For masonry unit properties, from section 4.2 of SIA 266:

$$f_{xk} = \frac{\gamma_m}{\eta_1 \eta_2} f_{xd} \quad (1)$$

where f_{xk} and f_{xd} are the characteristic and design strength values perpendicular to bed joints, respectively. γ_m is the partial factor taking into account the approximation of the resistance model, as well as the differences in material properties compared to their characteristic values. η_1 , on the other hand, is the conversion factor taking into account the decrease of f_{xd} in the header and stretcher masonry. Finally, η_2 is the conversion factor to consider the increase in f_{xd} in case of a solicitation of a localized area. From the same reference, for the benchmark buildings, $\gamma_m=2.0$, and $\eta_1=\eta_2=1.0$. Therefore:

$$f_k = 2 f_d \quad (2)$$

According to Eurocode6 (BS EN 1996-1-1:2005), characteristic values of masonry properties can be considered as the 5% percentile of the expected values. For a normal distribution of the material properties:

$$f_{xk} = X_{5\%} = \mu - 1.65\sigma \quad (3)$$

where μ and σ are the mean and standard deviation of the expected material properties. Considering a coefficient of variation (COV) of 0.2 (from literature), it is seen that:

$$\mu = 1.98 f_{xk} = 3.96 f_{xd} \quad (4)$$

Replacing the values in Table 2 in Equation 4, the expected masonry unit properties that are used in the dynamic analysis in this project are shown in Table 3. It should be noted that the elastic modulus for masonry is reduced by 50% to consider the cracking in the masonry units in the existing buildings (Lang 2002).

Table 3: Expected properties of masonry units used in the dynamic analyses

	CHB30	YVR14	SECH7	STD40
Masonry modulus of elasticity (GPa)	1.5	2.0	2.0	2.0
Compression strength (MPa)	10 (\perp bed joints) 4.2 (\perp head joints)	10 (\perp bed joints) 6.3 (\perp head joints)	10 (\perp bed joints) 6.3 (\perp head joints)	10 (\perp bed joints) 6.3 (\perp head joints)
Tensile strength (MPa)	0.75	1.0	1.0	1.0

Similar to masonry, average material properties derived from standard values are used for concrete and reinforcing steel.

3. Methodology

3.1. Progressive collapse in masonry structures

As the structural boundaries and load conditions generally prevent the masonry to fail in compression, the following types of failure (Figure 2) can occur in masonry units during an earthquake: (1) joint de-bonding, (2) units sliding along bed or head joints, and (3) units cracking under direct tension. These types of failure in masonry units can simulate in-plane and out-of-plane failure modes in masonry walls (piers and/or spandrels).

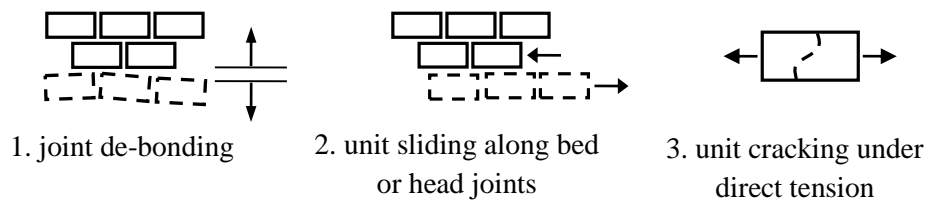


Figure 2: Failure modes in masonry units

In-plane damage mechanisms for masonry walls are governed by failure modes in flexure (rocking), shear sliding along the joints or shear diagonal cracking (Calderini et al. 2009). The occurrence of each of those failure modes depends on several parameters such as the wall boundary conditions, the axial load of the wall, and masonry geometrical characteristics and constituents. Several references discuss the tendency of the prevalence of each failure mode based on the condition/value of those parameters (e.g., Magenes and Calvi 1997; Bosiljkov et al. 2003). It should be noted that there is not always a crystal clear certainty of the occurrence of a specific failure mode because many interactions may happen between them. Failure will occur in piers or spandrels based on their relative stiffness and strength (Paulay and Priestley 1992; Belmouden and Lestuzzi 2007). In weak pier-strong spandrel, the plastic displacement due to flexure or shear will be concentrated in the piers of one storey (generally the first floor) which results in a soft storey mechanism in the building. In the other damage mechanism, strong pier-weak spandrel, the failure modes of spandrels can be rocking, usually occurring on top floors, or diagonal cracking, happening in mid-storeys (Cattari and Lagomarsino 2008).

The out-of-plane damage mechanism, on the other hand, is governed by the connection of the walls to the roof, floors, the intersecting walls, and the axial load level, and also the position and dimension of openings. Some of the most probable out-of-plane failure mechanisms are reported in (D'Ayala and Speranza 2002). To capture those failure mechanisms in the structural analysis stage, the Finite Element Method is somewhat known as the most common method to create a 3-D model of the structure.

In the context of the structural analysis of masonry buildings using a Finite-Element-based analysis, materials are modelled as a continuum, and elements are connected at nodes; therefore, it is assumed that all elements sharing the same node have the same displacement. However, to accurately track the behaviour of each element when element separation occurs in a progressive collapse analysis, elements should be considered to displace independently. An alternative is to use multiple node ID's at expected separation points; however, this technique can result in stress singularity and inaccurate stresses at locations of nodal separation which leads to an uncertain stress distribution within the whole structure. On the other hand, special techniques must be adapted to model cracks in the elements, and to consider the effect of element separation on the building's overall stiffness. One technique known as "smeared cracks" deals with cracks by considering their effect on stiffness and stress-strain equations (Cervera & Chiumenti 2006). Although showing considerable accuracy in calculating displacements and failure loads, models developed based on this method are relatively complicated. Moreover, special elements should be used in the location of dominant cracks (Tagel-Din & Meguro 2000). Such a method also requires previous knowledge of the location and direction of cracks' propagation. Nonetheless, in most cases, the fracture plane is arbitrary and unknown before the analysis. The same problem exists for

another technique known as “discrete cracks” modelling, in which cracks are taken into account as discrete items (Carol et al. 1997). The latter method is more appropriate for cases with few cracks.

The elastic (or elasto-plastic) FEM analyses has been applied in some researches for the seismic vulnerability assessment and rehabilitation of masonry buildings (Ismail et al. 2009). However, in those applications, the nonlinear behaviour of the materials and consequently, of the whole structure, in a progressive collapse simulation is missed; therefore, developing precise fragility curves for masonry buildings would be difficult through those methodologies.

3.2. Application of the AEM for masonry and reinforced concrete

To overcome the above problems, the Applied Element Method (AEM) is used in this project as an alternative to the FEM. This method, which is based on dividing structural members into virtual elements connected through springs (Figure 3), which means that there are no common nodes, can simulate large displacements and elements progressive separation through successive failure of those springs (Meguro and Tagel-Din 2002).

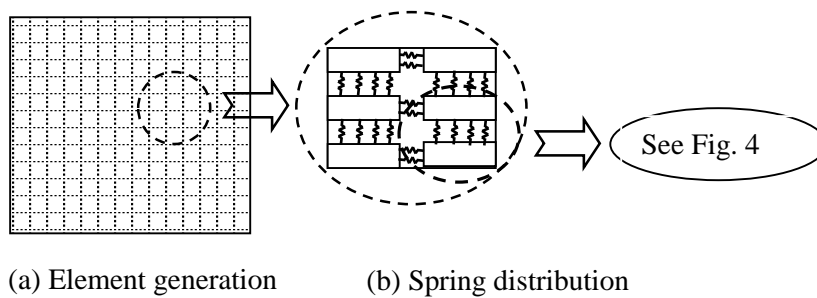


Figure 3: Modelling an element in AEM

The normal and shear springs located at the element contact points, distributed around the edges, as shown in Figure 3, represent stresses, strains, and deformations of certain portions of the structure. Figure 4 shows an example of the configuration of springs between two elements, extended from the centerline of one element to the centerline of the adjacent one. In that figure, a is the distance between the springs, d is the length of the represented area by each spring which is actually the element’s length, and t is the thickness of the element, respectively.

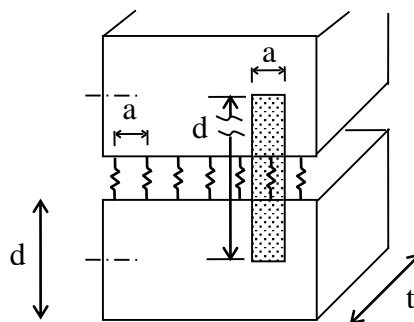


Figure 4: Spring distribution and area of influence of each springs pair in AEM
Adapted from (Mayorca and Megura 2003)

To apply the AEM method for masonry, two types of springs are needed to represent bricks and the brick-mortar interaction, as shown in Figure 5. If the crack passes through the bed or head joints, the brick-mortar springs are affected. On the other hand, if the crack passes directly through bricks, the failure is modelled using the failure of the brick springs.

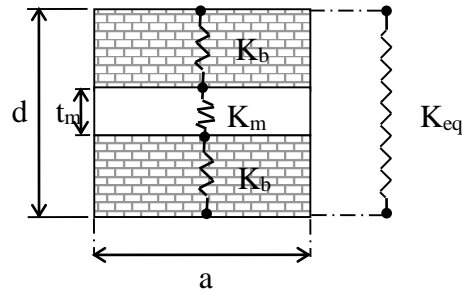


Figure 5: Modeling masonry in AEM

For the studied unreinforced masonry buildings, a total number of 5 springs is used on each face of the elements. The size of the meshing is selected to avoid creating elements with large aspect ratios. To this end, an approximate number of 22500 and 83500 elements are used for the buildings in Lausanne and Yverdon, respectively. As damage to the slabs is of less interest, in comparison to the masonry walls, a bigger meshing size is chosen for the concrete floors.

Several constitutive models are adopted in the Applied Element Method to model the concrete in compression. Before and after cracking as for modelling of concrete under compression, the Maekawa (Okamura and Maekawa 1991) compression model is adopted. In this model, three values are used to define the envelope for compressive stresses and compressive strains: the initial Young's modulus, the fracture parameter, representing the extent of the internal damage of concrete and the compressive plastic strain are introduced to define the envelope for compressive stresses and compressive strains. The tangent modulus is calculated according to the strain at the spring location. For concrete springs subjected to tension, spring stiffness is assumed as the initial stiffness until reaching the cracking point. After cracking, stiffness of springs subjected to tension is set to be zero. The residual stresses are then redistributed in the next loading step by applying the redistributed force values in the reverse direction. For concrete springs, the relationship between shear stress and shear strain is assumed to remain linear till the cracking of concrete. Then, the shear stresses drop down. The level of drop of shear stresses depends on the aggregate interlock and friction at the crack surface. For reinforcement springs, the Ristic (Ristic et al. 1986) model is used. In this model, the tangent stiffness of reinforcement is calculated based on the strain from the reinforcement spring, loading status (either loading or unloading) and the previous history of steel spring which controls the Bauschinger's effect. The main advantage of this model is that it can consider easily the effects of partial unloading and Bauschinger's effect without any additional complications to the analysis.

In a seismic vulnerability evaluation process, the calculated responses are sensitive to the characteristics of the individual ground motion used as the seismic input. Therefore, different ground motion records are required to obtain a good estimation of the building's responses. To apply the Applied Element Method in the nonlinear dynamic procedure, large deformations of an element under dynamic loads are calculated by the following general dynamic equation of motion (Tagel-Din and Meguro 2000).

$$[M][\Delta U'''] + [C][\Delta U'] + [K][\Delta U] = [\Delta f(t)] + [R_m] + [R_G] \quad (5)$$

In Equation 5, $[M]$ is the mass, $[C]$ is the damping, and $[K]$ is the stiffness matrix. Moreover, $\Delta f(t)$ is the incremental applied load vector, $[\Delta U]$ is the incremental displacement vectors, and $[\Delta U']$ and $[\Delta U'']$ are the incremental velocity and acceleration vectors, respectively. The vector R_m in Equation 5 stands for the residual forces caused by cracking, or the incompatibility between strains and stresses at the spring location due the nonlinear behaviour of materials. The vector R_G , on the other hand, represents the residual forces caused by geometrical changes of the structure during loading. In this regard, the AEM has an advantage over the FEM, noting that the latter considers the redistribution of internal forces resulting from geometrical changes by adopting a geometrical stiffness matrix. The nonlinear material behaviour in the AEM is taken into account in calculating $[K]$ and R_m .

3.3. Verification of AEM with experimental tests

Comparison of experimental tests results with AEM analytical results shows that AEM method has the ability to simulate in-plane and out-of-plane failure modes in masonry units and in masonry structures (Karbassi and Nollet 2013).

3.3.1. In-plane loading

Previous studies have shown good agreement between AEM analytical model results and experimental tests for the static loading of masonry walls from the linear range until the in-plane failure of the walls (Karbassi 2010; Mayorca and Meguro 2003). To illustrate the ability of AEM to simulate the behaviour of masonry walls under cyclic loading, results from the experiments carried out by Vasconcelos (2005) are compared here with AEM results. The 120 x 100 cm² wall with a 20 cm thickness (made of 25cm x 12cm x 5.5cm brick units) was subjected to a displacement-control cyclic loading with a displacement increment of 5mm. An additional pre-compression load corresponding to a stress level of $\sigma=125$ N/cm² was applied to the wall before applying the horizontal increasing displacements. Figure 6 shows the results from the AEM model and the envelope of the hysteresis curves from the experimental test. Figure 7 also shows the damage in the AEM model and the experimental test for this loading case. It is seen that the AEM model represents the in-plane cyclic behaviour of the experimental wall with a good degree of accuracy.

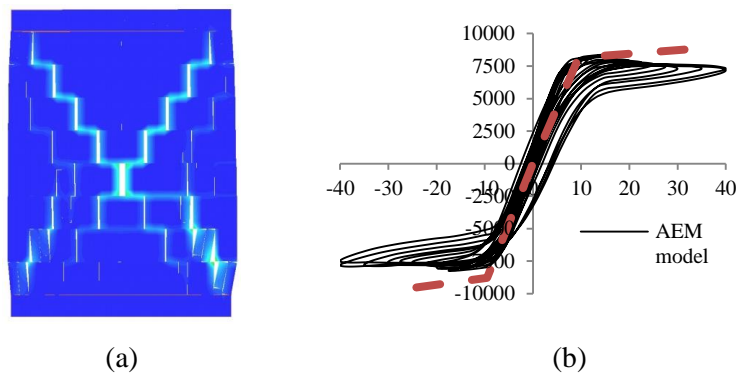


Figure 6: (a) Strain contours in the wall at the end of the cyclic load (b) comparison of the AEM model results and the experimental test for the in-plane cyclic loading



Figure 7: Comparison of damage in the AEM model and the experimental test for the in-plane cyclic loading

3.3.2. Out-of-plane loading

Comparison of AEM analysis results for the static out-of-plane loading of a masonry wall with experimental test (Sathiparan 2005) is shown in Figure 8. The 47.5x23.5 cm² wall with a 5 cm thickness

was subjected to a displacement-control out-of-plane line load at the mid-span on the wall. The loading rate was 0.05 mm/min. As seen in Figure 8, the force-displacement curve from the AEM analytical model represents the average behaviour observed from the experimental tests. Figure 9 also shows the comparison of the damage in the AEM model with the experimental test.

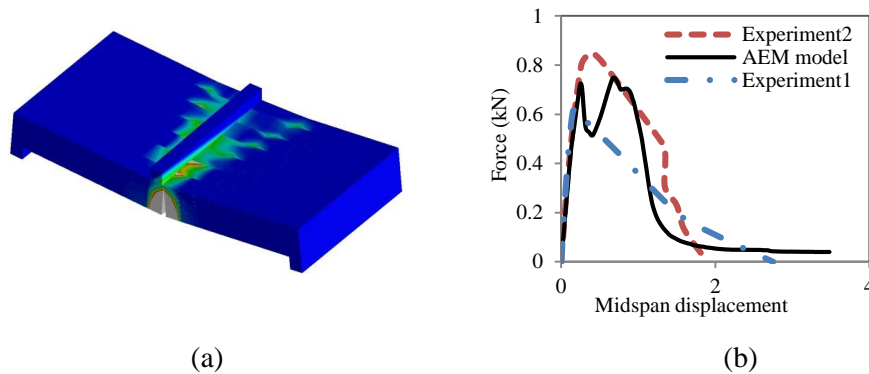


Figure 8: (a) Strain contours in the wall at the end of the static load (b) comparison of the AEM model results and the experimental test for the out of plane cyclic loading

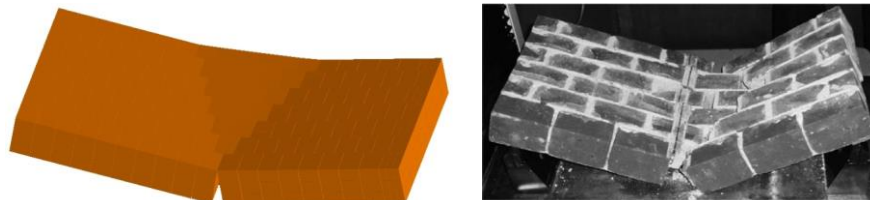


Figure 9: Comparison of damage in the AEM model and the experimental test for the out-of-plane static loading

Verification for dynamic loading case is performed through the comparison of AEM model with the impulse loading experimental tests for the wall in Griffith et al. (2004). The 150x100 cm² wall with an 11cm thickness was subjected to out-of-plane half-sine-wave impulse support motions. The support displacement impulse frequency ranged from 1 to 3 Hz. At each frequency, the impulse displacement amplitude (PGD) was gradually increased until out-of-plane rocking of the wall happened. Figure 10 shows the peak wall displacement at the mid-height vs. the impulse motion frequency. Each line in Figure 10 corresponds to a constant impulse displacement (PGD). A clear agreement among the analytical and experimental results is also seen in case.

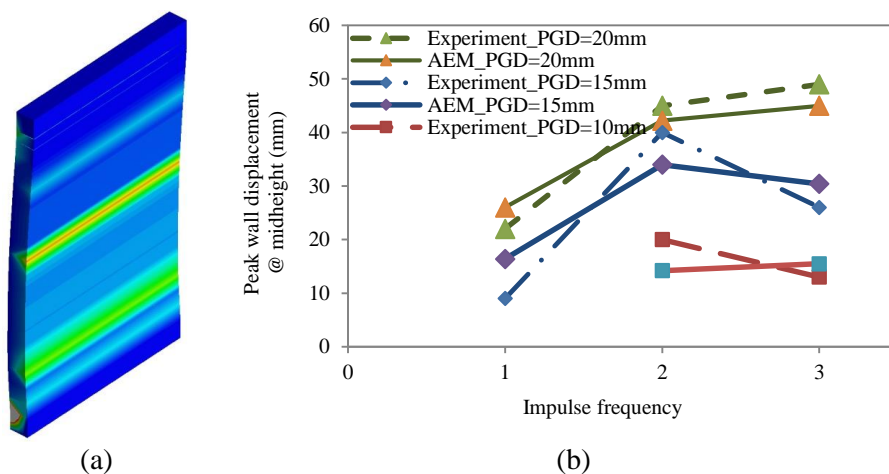


Figure 10: (a) Strain contours in the wall at the end of the impulse load (b) comparison of the AEM model results and the experimental test for the out-of-plane dynamic loading

3.3.3. Half-scale 4 storey RC-URM building

The AEM is used to numerically model the shake table test on a half-scale mixed 4-storey RC-URM building, which was conducted at the TREES laboratory of the Eucentre, Pavia, in Italy (Tondelli et al. 2013, Beyer et al. submitted, Tondelli et al. submitted). The test unit consisted of two RC and six URM walls and was subjected to uni-directional excitation at different levels of intensity. Figure 11 shows the test unit and the AEM numerical model.

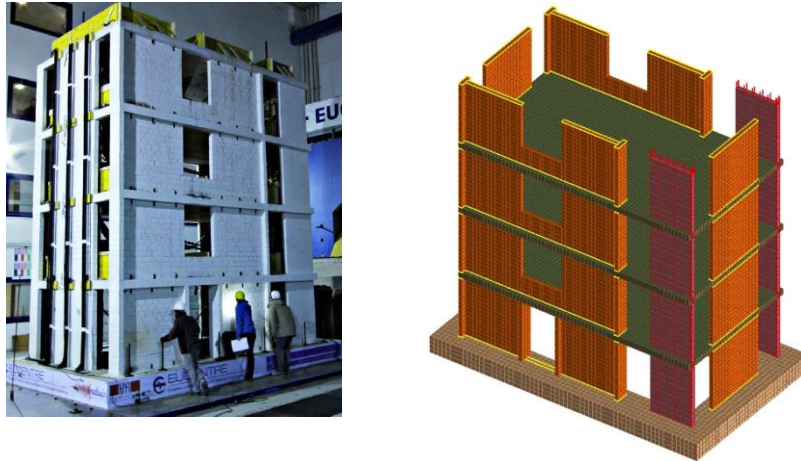
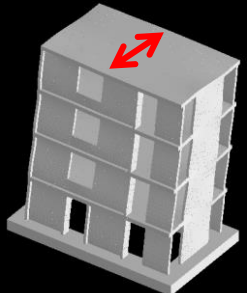


Figure 11: 4-storey mixed RC-URM building (half-scale) and the AEM numerical model

The connection between the URM walls and the concrete slabs in the model is governed by friction force (yellow regions in Figure 11). This means that there is no moment resistance at the interface of the URM walls and the RC slabs. This is also the case for the interface between the bottom of the URM walls in the first floor and the RC foundation. The RC foundation, however, has a fixed connection with the ground.

Table 4 shows the comparison of the periods of the first 3 modes of vibration that were detected in the numerical mode with the shake table test unit. The ground motion record used for the shake table test was the ground motion recorded at the HercegNovi station during the 1979 Montenegro earthquake. To account for the fact that the structure is constructed at half-scale, the record was scaled in time by reducing the duration by a factor $\sqrt{2}$. The record was base line corrected and then scaled to match the different levels of peak ground acceleration, 0.05g, 0.1g, 0.2g, 0.3g, 0.4g, 0.6g, 0.7g, 0.9g, that were used as input signals for the shake table test. In order to retain the damage consequence from each level of PGA to the next, as it happened in the shake table test, a continuous ground motion record input consisted of all the scaled records is created for the numerical model. A 30 second rest time (zero acceleration) is put in between each scaled record to model the rest time between tests in the shake table unit.

Table 4: Period of the first three modes of vibration

	Test unit (sec.)	AEM model (sec.)
	0.232	0.203

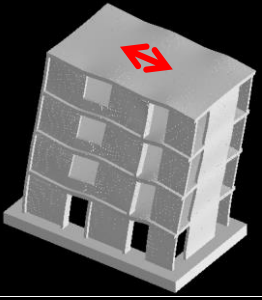
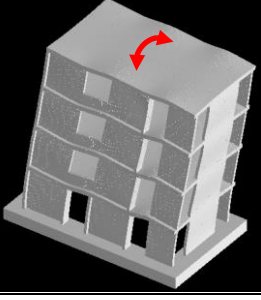
	0.128	0.121
	0.103	0.098

Figure 12 shows the comparison between the storey drift values of the test unit (solid line) and the numerical model (dash line) up to test 6 (PGA=0.6g), after which the numerical model collapses.

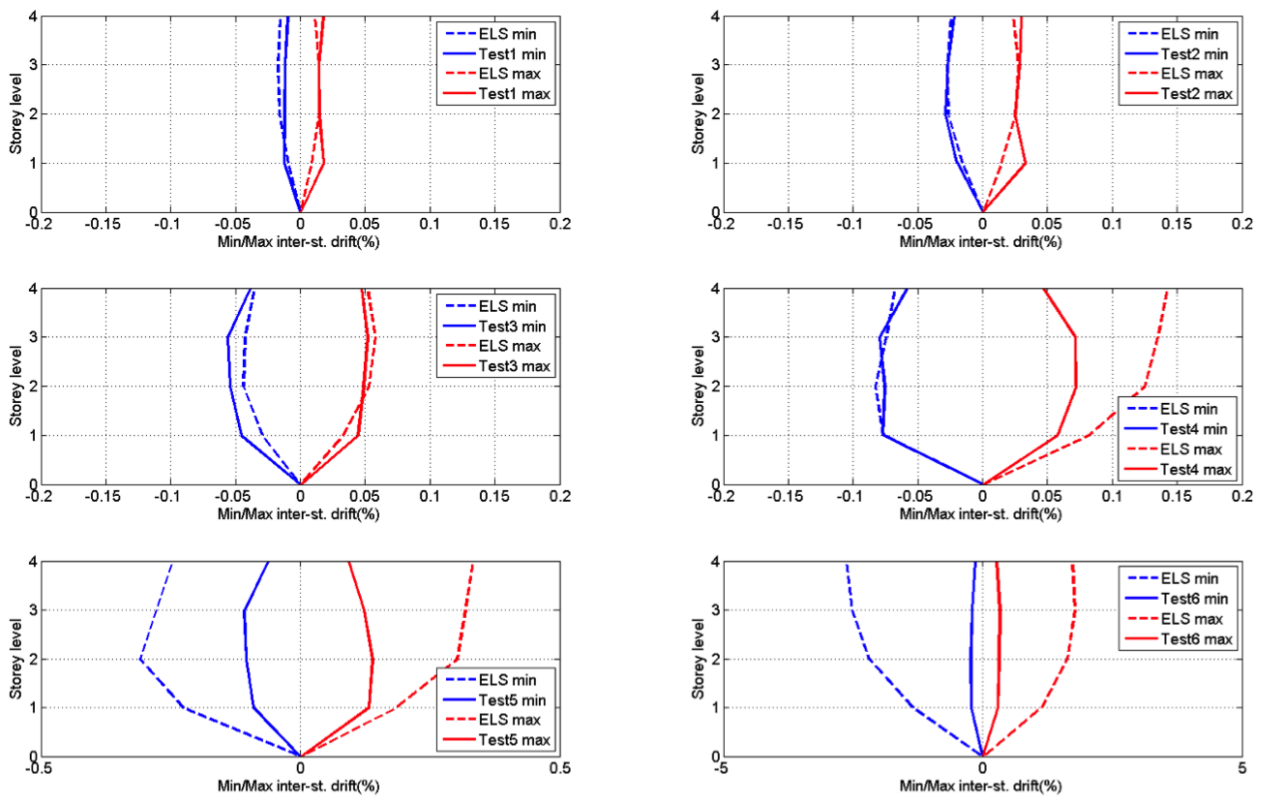


Figure 12: Comparison of the storey drift values between the test unit and the AEM numerical model

It is seen in this figure that up to test 3 (PGA=0.2g), there is a good agreement between the shake table test and the numerical model. The difference becomes more significant from test 4 (PGA=0.3g) as the numerical model gets close to the collapse point at test 6 (PGA=0.6g). One explanation for such a premature collapse could be the premature damage in the concrete foundation of the numerical model

in the higher intensities. Such damage would influence the behaviour of the structure, which could explain the premature failure of the model in comparison to the test unit. Figure 13 shows the state of the numerical model on the verge of collapse at test 6.



Figure 13: Collapse of the model during test 6 (PGA=0.6g)

Overall, it can be concluded that the AEM tool used in this study is in good agreement with the shake table test. However, for high damage grade the numerical model shows more conservative results when compared to the test.

3.4. Definition of damage grades in masonry and reinforced concrete buildings

To conduct the seismic vulnerability evaluation for the studied buildings in this project, a clear definition of the damage grades is essential. The EMS-98 (Grünthal 1998) damage grades are used in this research work to determine the limit states from the dynamic analysis. In this way, the obtained results would be in accordance with the existing EMS-based methodologies in Switzerland. Tables 4 and 5 present the description of those damage grades for masonry and reinforced concrete buildings, respectively.

Table 4: Description of the damage grades for URM buildings according to EMS-98






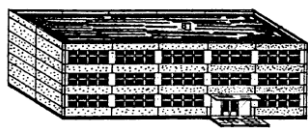
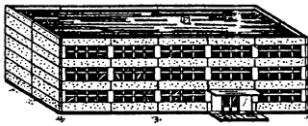



Damage Grade	Description of damages	
D1	Negligible to slight damage: no structural damage, slight non-structural damage: Hair-line cracks in very few walls. Fall of small pieces of plaster only. Fall of loose stones from upper parts of buildings in very few cases.	
D2	Moderate damage: slight structural damage, moderate non-structural damage: Cracks in many walls. Fall of fairly large pieces of plaster. Partial collapse of chimneys.	
D3	Substantial to heavy damage: moderate structural damage, heavy non-structural damage: Large and extensive cracks in most walls. Roof tiles detach. Chimneys fracture at the roof line; failure of individual non-structural elements (partitions, gable walls).	
D4	Very heavy damage: heavy structural damage, very heavy non-structural damage: Serious failure of walls; partial structural failure of roofs and floors.	
D5	Destruction: very heavy structural damage. Total or near total collapse.	

Table 5: Description of the damage grades for RC buildings according to EMS-98

Damage Grade	Description of damages	
D1	Negligible to slight damage: no structural damage, slight non-structural damage. Fine cracks in plaster over frame members or in walls at the base. Fine cracks in partitions and in-fills.	
D2	Moderate damage: slight structural damage, moderate non-structural damage. Cracks in columns and beams of frames and in structural walls. Falling mortar from the joints of wall panels.	
D3	Substantial to heavy damage: moderate structural damage, heavy non-structural damage. Cracks in columns and beam column joints of frames at the base and at joints of coupled walls. Large cracks in partition and infill walls, failure of individual infill panels.	
D4	Very heavy damage: heavy structural damage, very heavy non-structural damage. Large cracks in structural elements with compression failure of concrete and fracture of rebars; tilting of columns. Collapse of a few columns or of a single upper floor.	
D5	Destruction: very heavy structural damage. Collapse of ground floor or parts (e. g. wings) of buildings.	

As the descriptions in Tables 4 and 5 are qualitative and depend on the engineering judgment, interpretations for those damage grades in Lang (2002) are used as shown in Tables 6 and 7. Consequently, material properties in Table 3 are used to determine damage grades in the dynamic analyses.

Table 6: Description of EMS-98 damage grades for URM according to Lang (2002)

Damage Grade	Description of damages
D1	First wall reaching the onset of cracking
D2	First wall reaching the yield displacement
D3	Slope of the capacity curve tends to zero (yielding in majority of walls)
D4	Failure of the first wall
D5	Drop of the capacity curve to 80% of the maximum value

Table 7: Description of EMS-98 damage grades for RC according to Lang (2002)

Damage Grade	Description of damages
D1	First wall reaching the onset of cracking
D2	First wall reaching the yield displacement
D3	Displacement corresponding to the yield of the last RC element.
D4	Failure of the first RC wall
D5	Drop of the capacity curve to 80% of the maximum value

3.5. Selection of the ground motion records

The ground motion records used in this project are chosen from the European ground motion record database with a condition of selecting those records which have spectral acceleration values covering the range of the spectral acceleration values provided by the Swiss Seismological Service for different cities in Switzerland. Table A-1 (appendix) presents the characteristics of the ground motion records used in the dynamic analyses of this research. The number of the analyses is more than the number of the ground motion records as in some cases, a magnified version of the ground motion records have been used to obtain damage grades 4 and 5 in the studied buildings. It should be noted that the duration stated in Table A-1 for each ground motion record is the length of the record that has been used in the nonlinear dynamic analysis. Figure 11 illustrates the distribution of the magnitude-distance to site for the ground motion records in Table A-1.

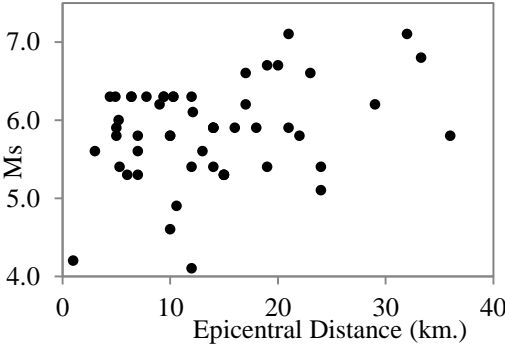


Figure 11: Magnitude-distance distribution of the ground motion records

The magnitude-distance distribution of the records is plausible for the seismicity of Switzerland, although the chosen set is statistically on the conservative side when compared with the hazard de-aggregation for Switzerland. This issue is due to the fact that relatively strong earthquake records are needed to reach damage grade 5 for all studied buildings. However, the magnitude does not exceed the value of Ms = 7 which is considered as still plausible for Switzerland.

3.6. Numerical model for the studied buildings

The nonlinear dynamic analyses in this paper are performed using an Applied Element-based method (Applied Science International, 2007). For both the unreinforced masonry and reinforced concrete elements, a total number of 5 springs is used on each face of the elements. The size of the meshing is selected to create elements between 10 and 20 cm in dimension. Figure 12 shows the numerical models for each of the buildings in Figure 1.

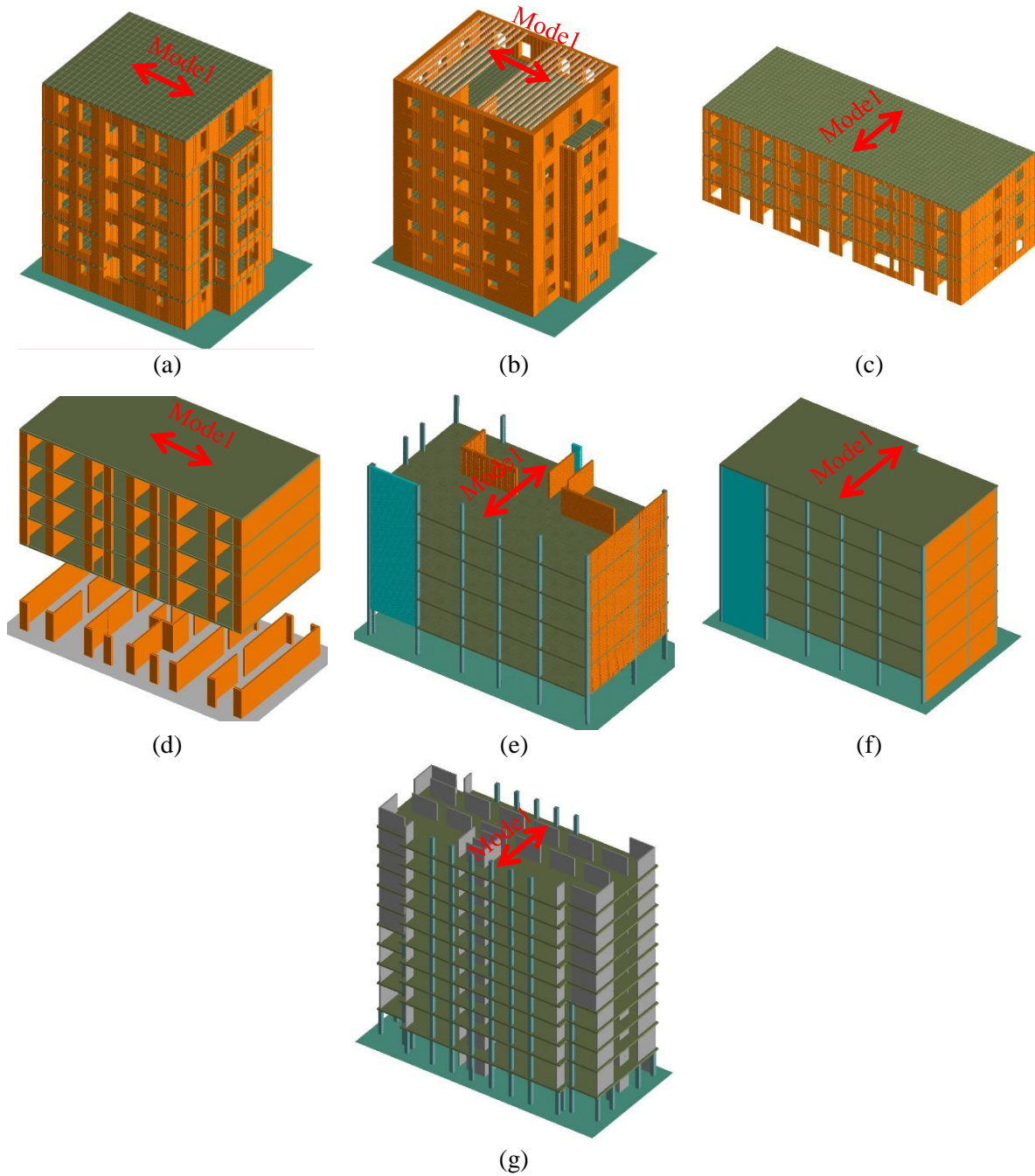


Figure 12: Numerical models using the AEM-based method (a) CHB30, (b) CHB30 ORG, (c) YVR14, (d) SECH7, (e) STD40 ORG, (f) STD40, and (g) SUVA

Table 8 presents the modal periods of vibration for each building.

Table 8: Modal periods of vibration for the studied buildings, T_1

	CHB30	CHB30 ORG	YVR14	SECH7	STD40 ORG	STD40	SUVA
1 st mode (sec.)	0.33	0.34	0.22	0.97	0.97	0.95	0.88
2 nd mode (sec.)	0.31	0.32	0.2	0.37	0.55	0.48	0.68

3.6.1. Boundary condition for the numerical models

The connection of the numerical models to the base is considered to be fixed. However, as this work does not consider the soil-structure interaction, the soil interface is considered an elastic material with the properties shown in Table 9.

Table 9: Elastic material used as the ground for the numerical models

E_e Young's modulus (GPa)	2
G_s shear modulus (GPa)	0.8
Friction coefficient	0.8

These values are representative of median soil conditions.

3.6.2. Input of ground motions

Both components X and Y of the records were used simultaneously in the 3D dynamic analysis. The component with the highest value of the spectral acceleration was systematically oriented parallel to the weakest direction (see Figure 12) of the studied building.

3.7. Development of fragility curves

The main objective of IMAC workgroup is to develop fragility curves for the studied buildings to be presented to Risk & Safety workgroup for seismic risk evaluation. The fragility curve for a building presents the probability of exceeding a damage grade DG, given engineering demand parameter EDP (e.g., spectral acceleration or spectral displacement). Therefore, the fragility curves for the buildings here are presented in the form of a two-parameter lognormal distribution function as follows.

$$F(X) = P(d > D) = \Phi \left[\frac{\ln(X) - \mu}{\sigma} \right] \quad (6)$$

In Equation 6, Φ is the standard normal cumulative distribution function, X is the distributed engineering demand parameter (e.g., S_a), and μ and σ are the median and standard deviation of the natural logarithm of the engineering demand parameters, respectively. As the available hazard data in Switzerland is in the form of spectral acceleration values, S_a is used in this report as the engineering demand parameter for the fragility curves.

It should be noted that the only uncertainty considered in developing the fragility curves in this report is the uncertainty related to the record-to-record variability. Such an uncertainty is taken into account by applying the ground motion record in Table A-1, in the dynamic analysis. The other sources of uncertainties related to AEM modelling parameters and mechanical material properties are conducted for one of the benchmarks and the results are reported separately in Section 4.

In order to compare the final risk calculations in this project with those performed by the practicing engineers in Switzerland, the spectral acceleration values used to develop the fragility curves are those calculated at the average period of each building corresponding to damage grade 2.

4. Results of dynamic analyses

4.1. Identification of damage grades

To identify the damage grades for each ground motion record, the descriptions in Table 5 are used in combination with the visual features of the Extreme Loading for Structures software. Damage grade 1 occurs when first tensile cracking happens in a wall. The stress contour of the buildings in Figure 13 shows an example of this damage grade. The blue color (in masonry) and black (in RC) show places where the stress value in the masonry walls has passed the tensile strength of the wall.

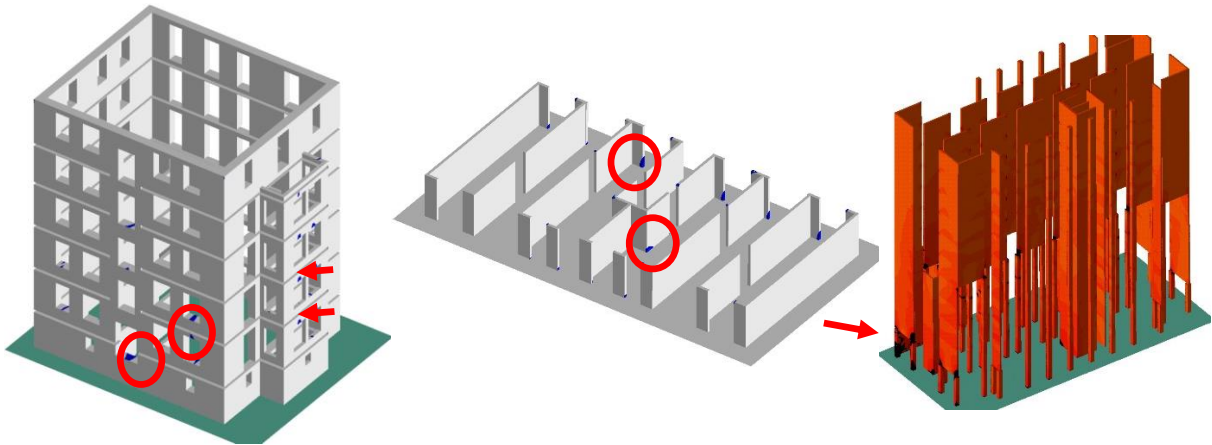


Figure 13: Stress contour in the buildings CHB30, SECH7, and SUVA showing damage grade 1

When the first wall in the building reaches the yielding point, the building has reached damage grade 2. Figure 14 shows an example of damage grade 2 in the building in Yverdon. The red spots on the walls in the first floor shows places at which the compressive strength has passed the limits stated in Table 3.

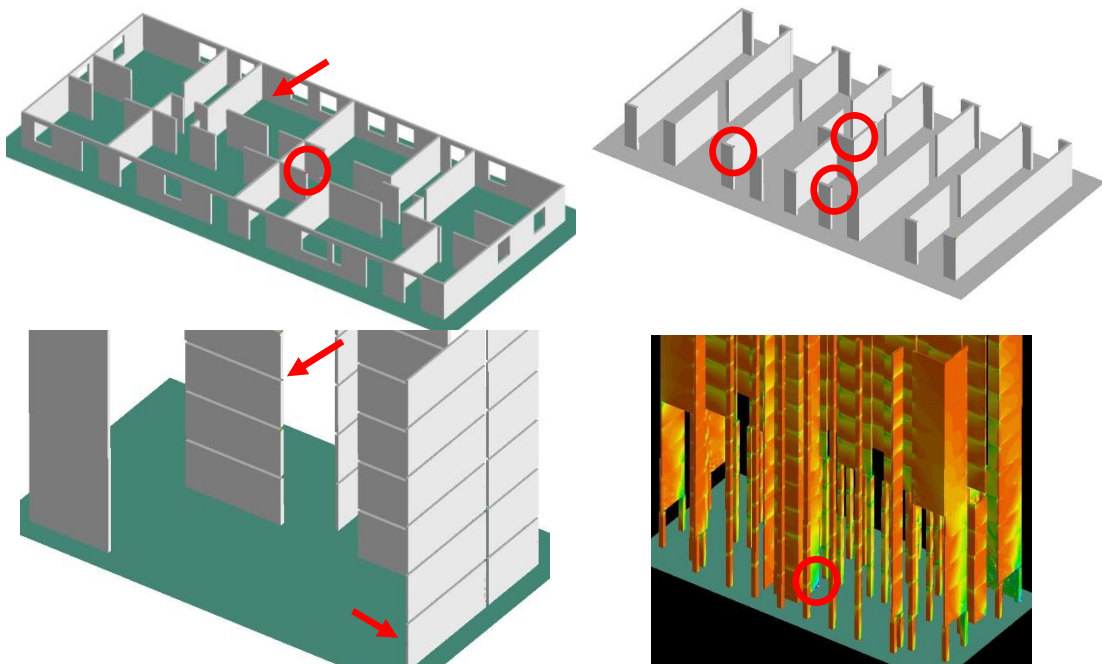


Figure 14: Stress contour in the buildings YVR14, SECH7, STD40 ORG, and SUVA showing damage grade 2

As stated in Tables 6 and 7, damage grade 3 happens when yielding occurs in the majority of walls in a building. Such a state is shown in Figure 15.

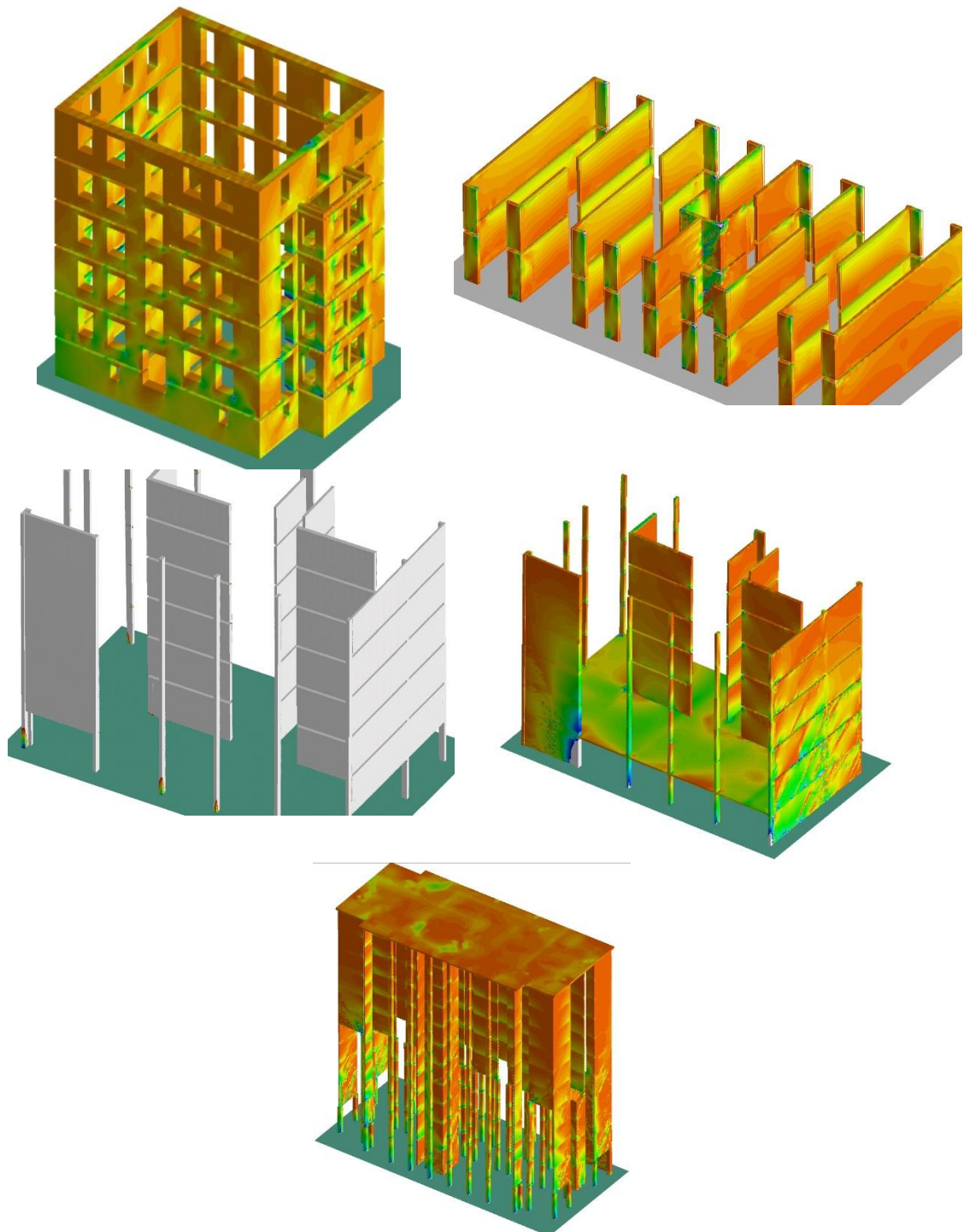


Figure 15: Stress contour in the buildings CHB30, SECH7, STD40 ORG, STD40, and SUVA showing damage grade 3

The damage grade 4 happens when the first or more walls in the studied buildings collapse. Figure 16 shows an example of such state.

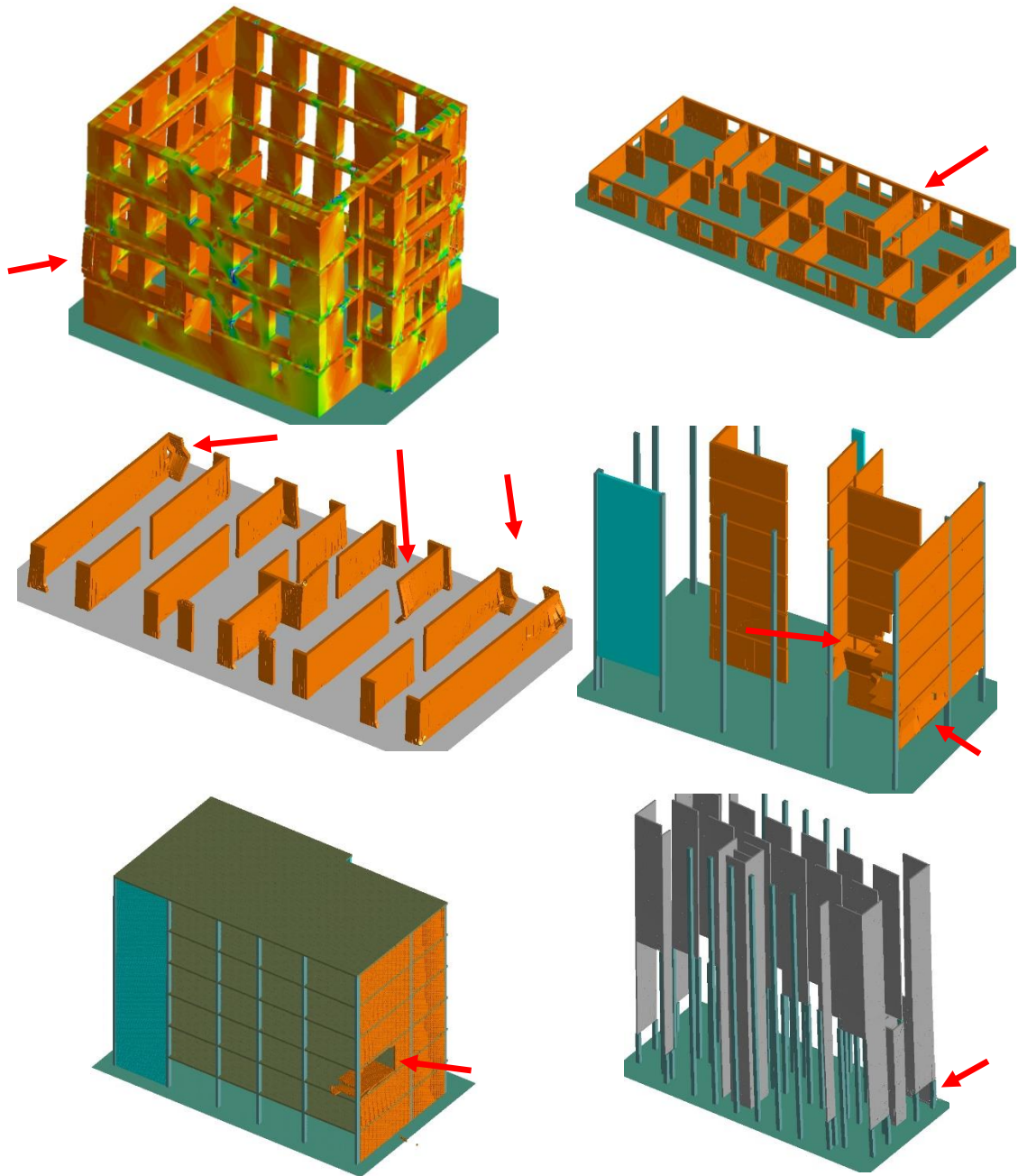


Figure 16: Collapse of the wall(s) as an indication of reaching damage grade 4 in CHB30, YVR14, SECH7, STD40 ORG, STD40, and SUVA

Damage grade 5, as stated in Tables 6 and 7 happens when the building is on the edge of total collapse or has been destroyed heavily. Figures 17 shows examples of damage grade 5.

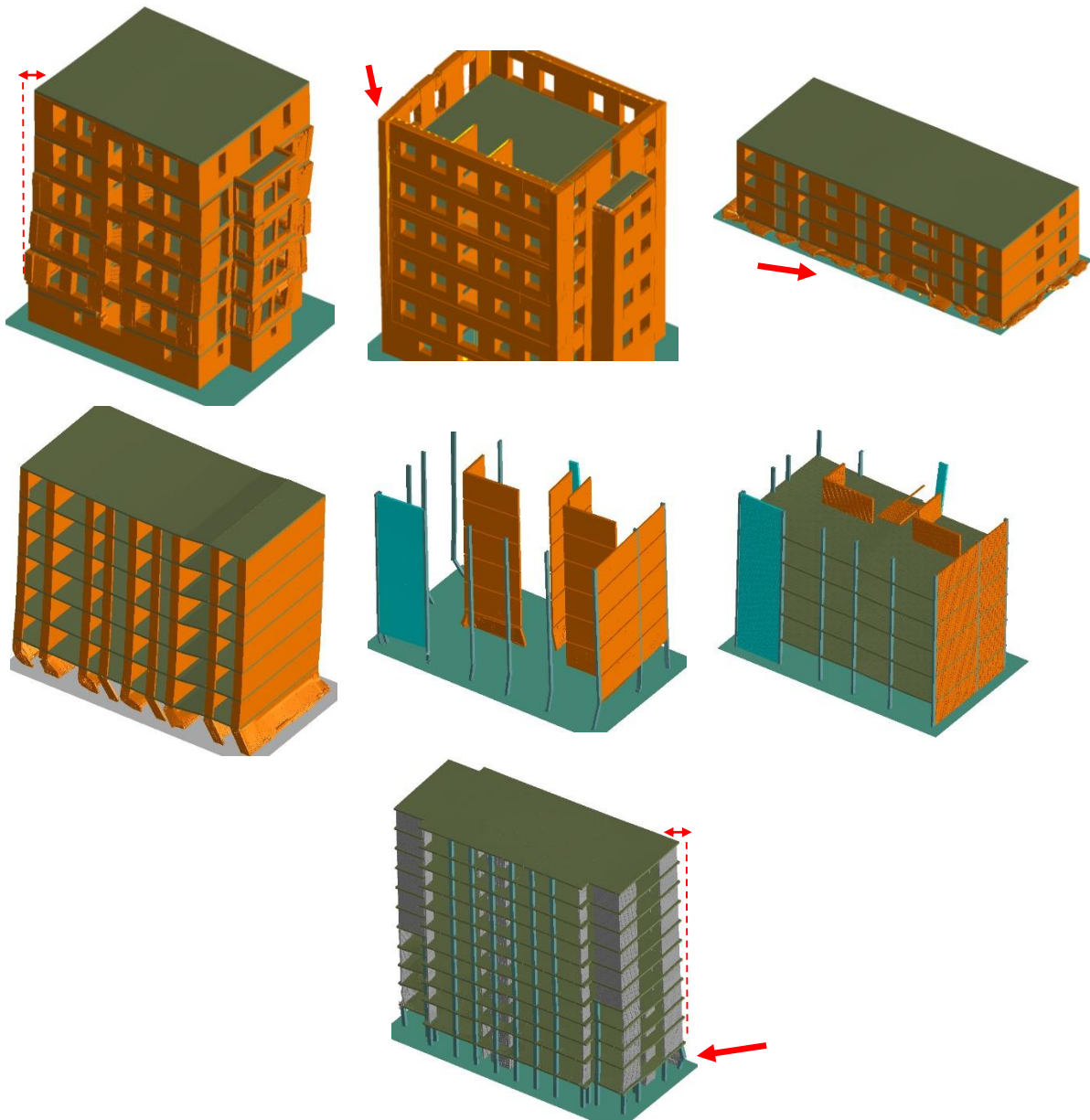


Figure 17: Damage grade 5 state in the studied buildings CHB30, CHB30 ORG, YVR14, SECH7, STD40 ORG, STD40, SUVA

Damage grade 5 is a result of soft storey in almost all the buildings except CHB30 ORG which collapse as a result of an out-of-plan mechanism.

4.2. Progressive change of modal period with damage

One feature of the AEM-based tool used in this work to study a few representative masonry and RC buildings in Switzerland, shown in Figure 1, is its capability of recording the change in the modal vibration period with progressive damage in the structure, for each ground motion record. Example of such a progressive change is shown in Figure 18 for the buildings SUVA. The X-axis in this figure corresponds to the length of the ground motion record, and the Y-axis shows the change in the period of the second mode of vibration.

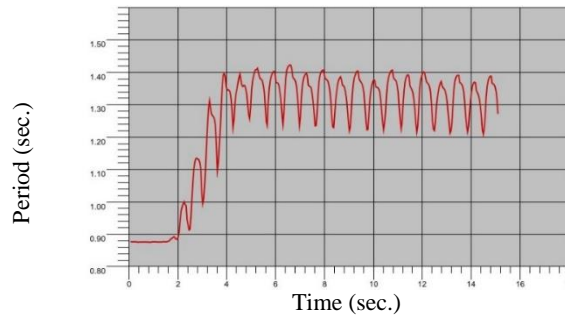


Figure 18: Example of the progressive change of period with damage for building SUVA

4.3. Results for the building CHB30

A total number of 61 3D-dynamic analyses were performed for the building CHB30 using the ground motion records in Table A-1. Figure 19 shows the distribution of the damage grades with the spectral acceleration (calculated at the modal periods of vibration, T_1 Table 8) of the ground motion records.

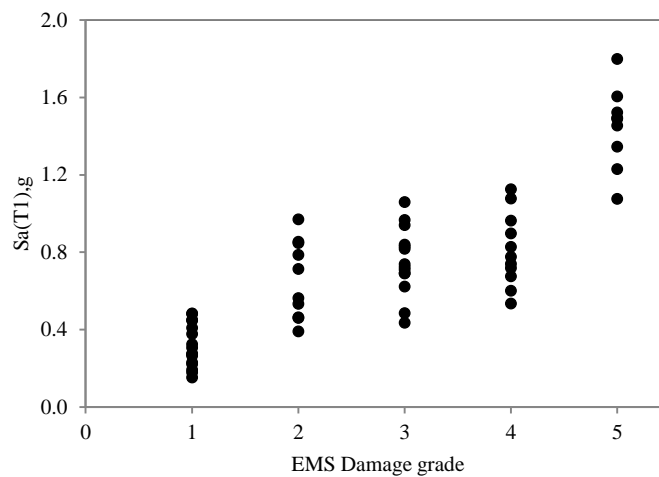


Figure 19: Distribution of the damage grades in CHB30 with the geometrical mean of the elastic spectral acceleration values

As both components of the records were used simultaneously in the dynamic analysis, it was not obvious at first to determine which spectral value should be used for the representation of the results for the fragility curves. After several trials, the geometrical mean of the spectral acceleration values from both X and Y directions appeared to be the most adequate value. $S_a(T_1)$ in Figure 19 and all the similar figures afterwards corresponds therefore to the geometrical mean of the spectral acceleration. The geometrical mean represents well the seismic demand in the fragility analysis of the studied buildings from a 3D analysis because it considers the magnitude of the spectral acceleration in both directions.

In simple methods used by practicing engineers, a reduction factor is applied to the module of elasticity to incorporate the cracking effect (similar to damage grade 2) in the material. There is no need to apply such a reduction factor in this study because the cracking in masonry and concrete is already incorporated through the progressive failure of the springs connecting the elements. However, in order to compare the final risk calculations in this project with those performed by the practicing engineers in Switzerland, the spectral acceleration values used to develop the fragility curves are those calculated at the average period of each building corresponding to damage grade 2. Those periods, shown in Table 10, are the average of the maximum progressive period experienced by each building from those ground motion records that cause damage grade 2. The related results are shown in Figure 20 for the building CHB30. In the next sections, the results of the distribution of the damage grades for all buildings are plotted for both the elastic T_1 (Table 8) and the T_{DG2} (Table 10) spectral acceleration values.

Table 10: Average modal periods of vibration for damage grade 2, T_{DG2}

	CHB30	CHB30 ORG	YVR14	SECH7	STD40 ORG	STD40	SUVA
1 st mode (sec.)	0.63	0.57	0.29	1.16	1.29	1.37	1.27
2 nd mode (sec.)	0.52	0.46	0.24	0.47	0.73	0.68	0.98

Figure 20 shows the distribution of the spectral acceleration values (calculated at the average modal periods of vibration of CHB30 building for damage grade 2, T_{DG2} Table 10) with the damage grades. The lognormal distribution of the data in Figure 20 is used later to develop the fragility curves for the building.

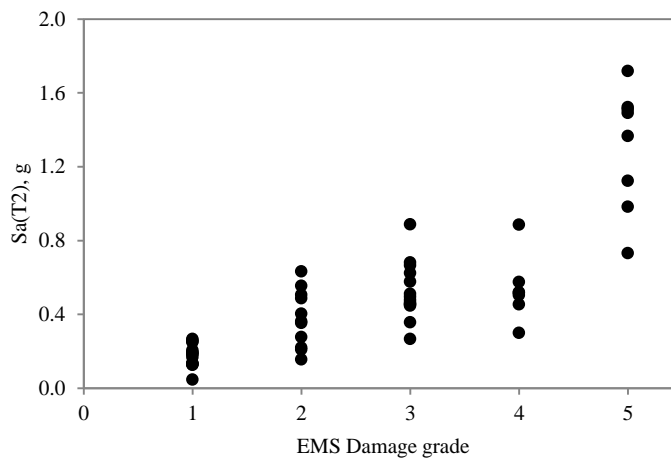


Figure 20: Distribution of the damage grades in CHB30 with the geometrical mean of the T_{DG2} spectral acceleration values

4.4. Results for the building CHB30 ORG

A total number of 51 3D-dynamic analyses were performed for the building CHB30 ORG using the ground motion records in Table A-1. Figure 21 shows the distribution of the damage grades with the spectral acceleration (calculated at the modal periods of vibration, T_1 Table 8) of the ground motion records.

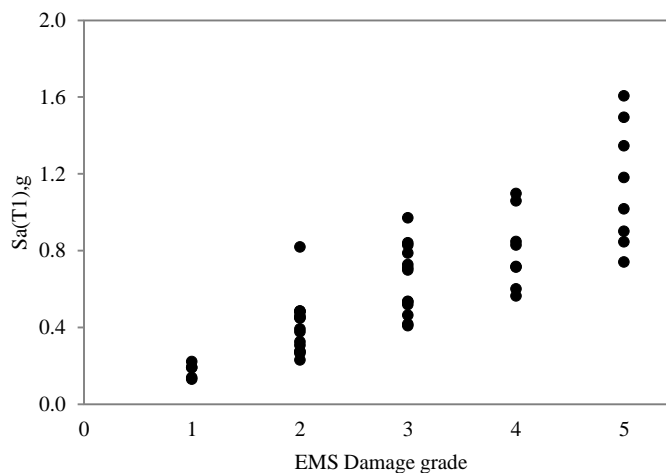


Figure 21: Distribution of the damage grades in CHB30 ORG with the geometrical mean of the elastic spectral acceleration values

The distribution of the spectral acceleration values (calculated at the average modal periods of vibration of CHB30 ORG building for damage grade 2, T_{DG2} Table 10) with the damage grades is shown in Figure 22. The lognormal distribution of the data in Figure 22 is used later to develop the fragility curves for this building.

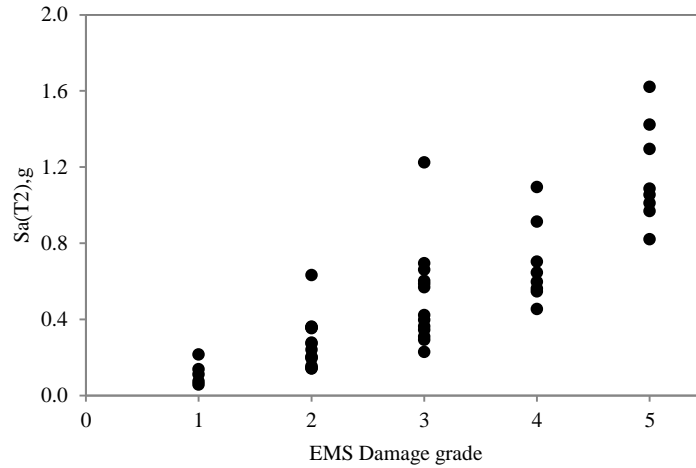


Figure 22: Distribution of the damage grades in CHB30 ORG with the geometrical mean of the T_{DG2} spectral acceleration values

4.5. Results for the building YVR14

A total number of 74 3D-dynamic analyses were conducted for the building YVR14 using the ground motion records in Table A-1. The distribution of the damage grades with the spectral acceleration (calculated at the modal periods of vibration, T_1 Table 8) of the ground motion records is shown in Figure 23.

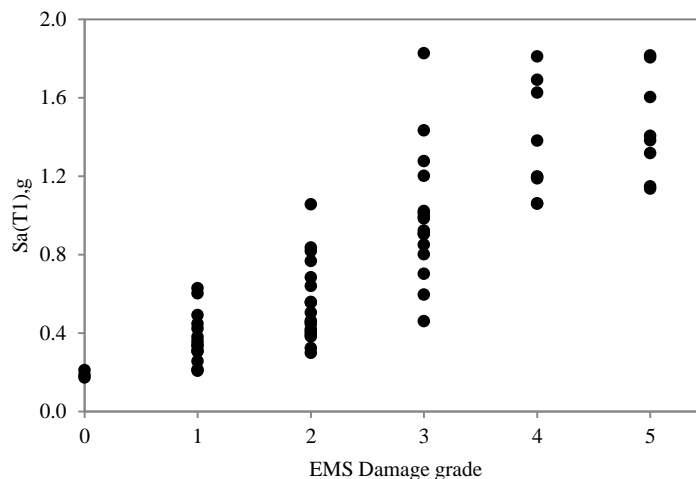


Figure 23: Distribution of the damage grades in YVR14 with the geometrical mean of the elastic spectral acceleration values

The distribution of the spectral acceleration values (calculated at the average modal periods of vibration of YVR14 building for damage grade 2, T_{DG2} Table 10) with the damage grades is shown in Figure 24. The lognormal distribution of the data in Figure 24 is used later to develop the fragility curves for this building.

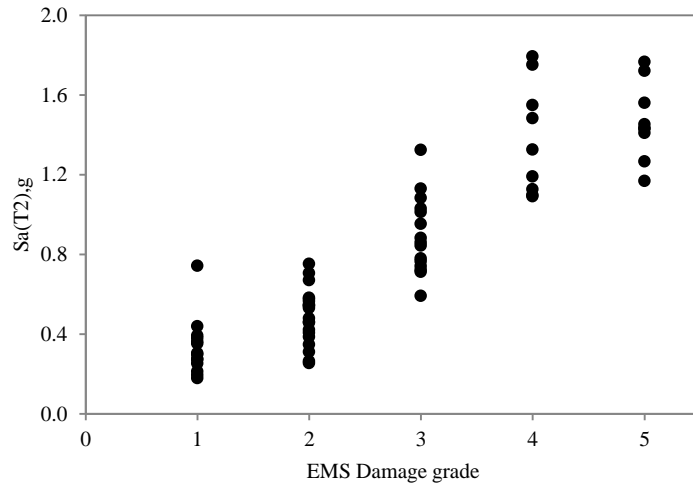


Figure 24: Distribution of the damage grades in YVR14 with the geometrical mean of the T_{DG2} spectral acceleration values

4.6. Results for the building SECH7

A total number of 55 3D-dynamic analyses were conducted for the building SECH7 using the ground motion records in Table A-1. The distribution of the damage grades with the spectral acceleration (calculated at the modal periods of vibration, T_1 Table 8) of the ground motion records is shown in Figure 25.

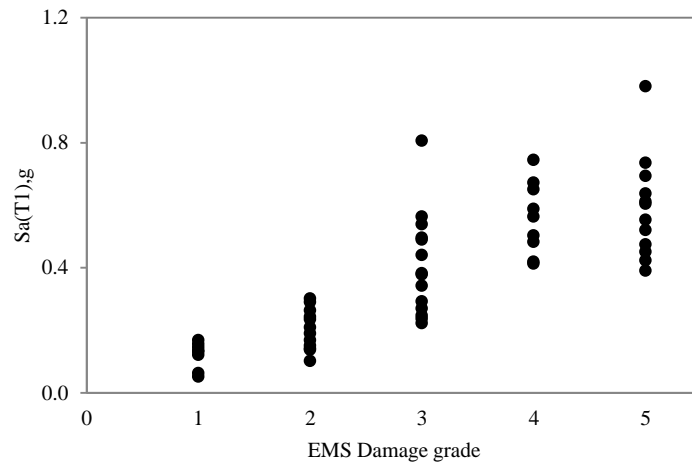


Figure 25: Distribution of the damage grades in SECH7 with the geometrical mean of the elastic spectral acceleration values

The distribution of the spectral acceleration values (calculated at the average modal periods of vibration of SECH7 building for damage grade 2, T_{DG2} Table 10) with the damage grades is shown in Figure 26. The lognormal distribution of the data in Figure 26 is used later to develop the fragility curves for this building.

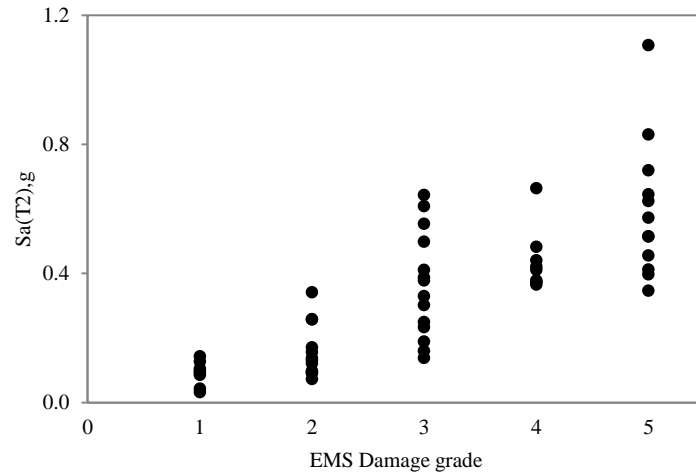


Figure 26: Distribution of the damage grades in SECH7 with the geometrical mean of the T_{DG2} spectral acceleration values

4.7. Results for the building STD40 ORG

A total number of 51 3D-dynamic analyses were conducted for the building STD40 ORG using the ground motion records in Table A-1. The distribution of the damage grades with the spectral acceleration (calculated at the modal periods of vibration, T_1 Table 8) of the ground motion records is shown in Figure 27.

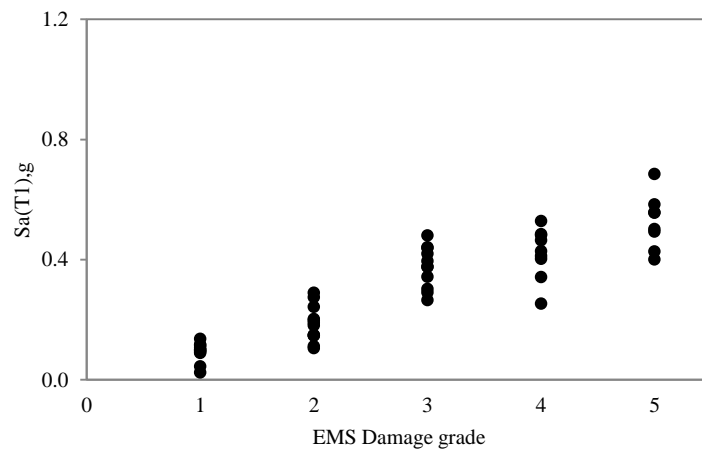


Figure 27: Distribution of the damage grades in STD40 ORG with the geometrical mean of the elastic spectral acceleration values

The distribution of the spectral acceleration values (calculated at the average modal periods of vibration of STD40 ORG building for damage grade 2, T_{DG2} Table 10) with the damage grades is shown in Figure 28. The lognormal distribution of the data in Figure 28 is used later to develop the fragility curves for this building.

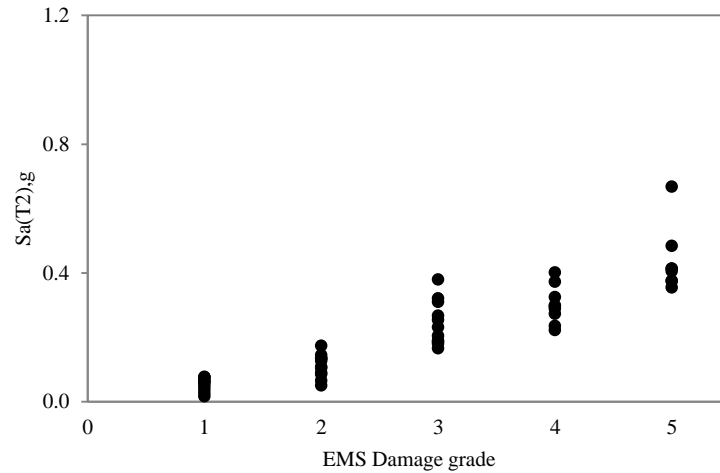


Figure 28: Distribution of the damage grades in STD40 ORG with the geometrical mean of the T_{DG2} spectral acceleration values

4.8. Results for the building STD40

A total number of 50 3D-dynamic analyses were conducted for the building STD40 using the ground motion records in Table A-1. The distribution of the damage grades with the spectral acceleration (calculated at the modal periods of vibration, T_1 Table 8) of the ground motion records is shown in Figure 29.

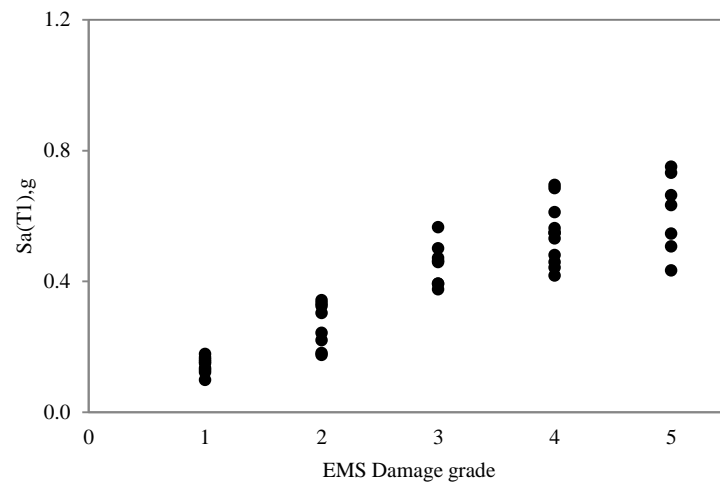


Figure 29: Distribution of the damage grades in STD40 with the geometrical mean of the elastic spectral acceleration values

The distribution of the spectral acceleration values (calculated at the average modal periods of vibration of STD40 building for damage grade 2, T_{DG2} Table 10) with the damage grades is shown in Figure 30. The lognormal distribution of the data in Figure 30 is used later to develop the fragility curves for this building.

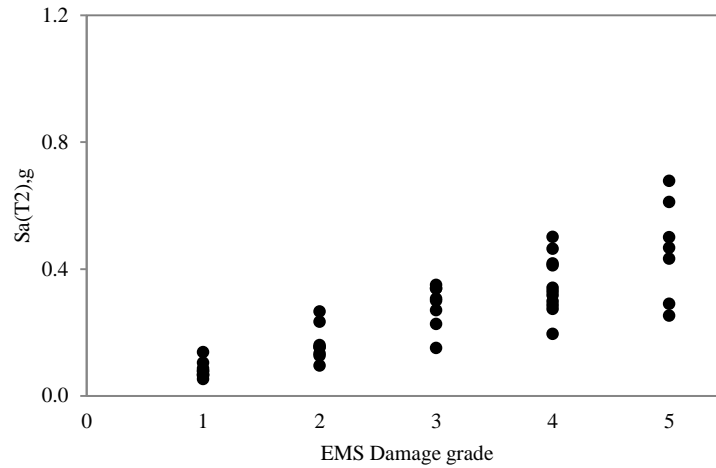


Figure 30: Distribution of the damage grades in STD40 with the geometrical mean of the T_{DG2} spectral acceleration values

4.9. Results for the building SUVA

A total number of 49 3D-dynamic analyses were conducted for the building SUVA using the ground motion records in Table A-1. The distribution of the damage grades with the spectral acceleration (calculated at the modal periods of vibration, T_1 Table 8) of the ground motion records is shown in Figure 31.

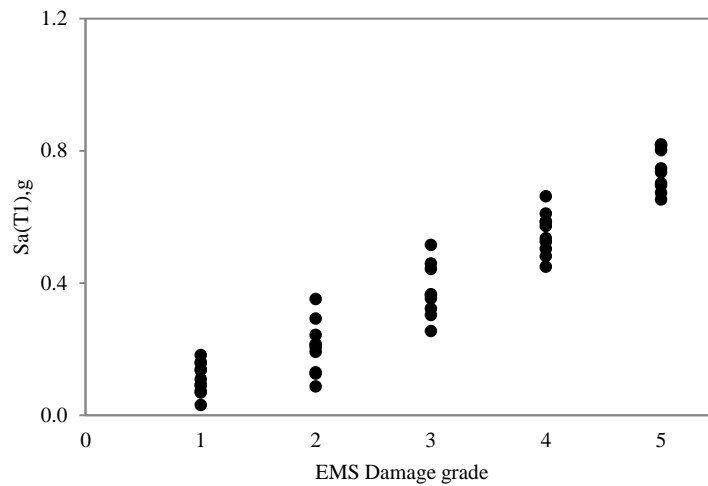


Figure 31: Distribution of the damage grades in SUVA with the geometrical mean of the elastic spectral acceleration values

The distribution of the spectral acceleration values (calculated at the average modal periods of vibration of SUVA building for damage grade 2, T_{DG2} Table 10) with the damage grades is shown in Figure 32. The lognormal distribution of the data in Figure 32 is used later to develop the fragility curves for this building.

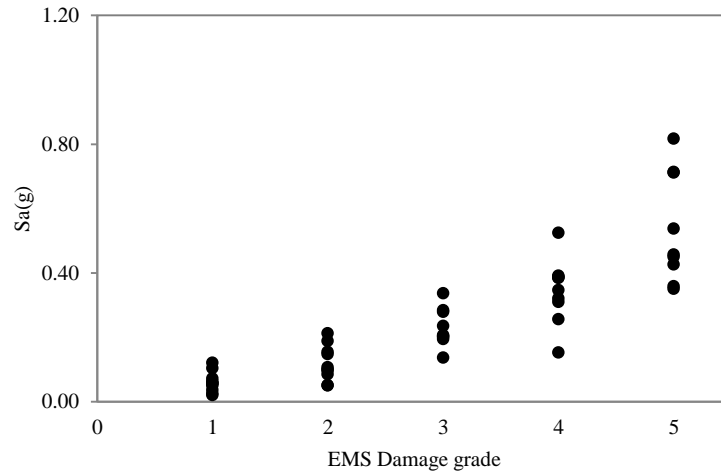


Figure 32: Distribution of the damage grades in SUVA with the geometrical mean of the T_{DG2} spectral acceleration values

4.10. Fragility curves of the benchmark buildings

The median and the standard deviation of the spectral acceleration values of ground motion records for each damage grade is calculated from Figures 20, 22, 24, 26, 28, 30, and 32. Using Equation 6, the fragility curves are presented in the form of a two-parameter lognormal distribution function.

4.10.1. Fragility curves for CHB30

Using the information in Figure 20, the median and standard deviation (for each damage grade) of the spectral acceleration values at the average maximum period for damage grade 2 (T_{DG2} , Table 10) for CHB30 is calculated and shown in Table 11.

Table 11: Median and standard deviation values of the intensity measures for the damage grades for CHB30

	Median (μ),g	Standard deviation (σ)
DG1	0.19	0.06
DG2	0.36	0.16
DG3	0.49	0.15
DG4	0.58	0.29
DG5	1.37	0.33

Using Equation 6 and the values in Table 11, the fragility curves for CHB30 is developed and presented in Figure 33.

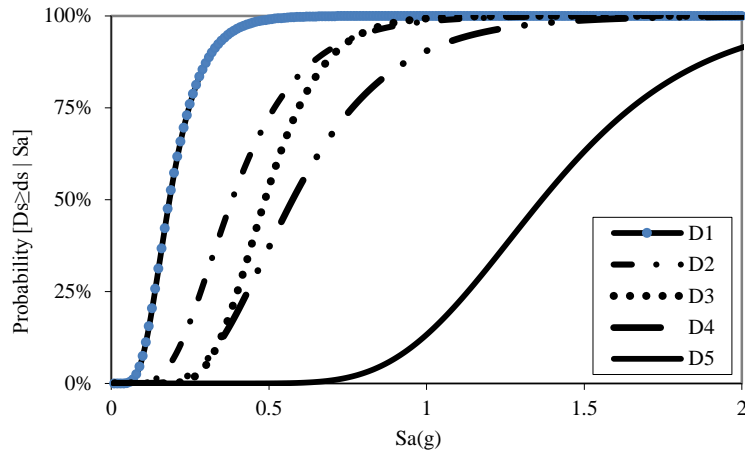


Figure 33: Fragility curves for CHB30

4.10.2. Fragility curves for CHB30 ORG

Using the information in Figure 22, the median and standard deviation (for each damage grade) of the spectral acceleration values at the average maximum period for damage grade 2 (T_{DG2} , Table 10) for CHB30 ORG is calculated and shown in Table 12.

Table 12: Median and standard deviation values of the intensity measures for the damage grades for CHB30 ORG

	Median (μ),g	Standard deviation (σ)
DG1	0.11	0.06
DG2	0.24	0.13
DG3	0.42	0.26
DG4	0.62	0.21
DG5	1.10	0.30

Using Equation 6 and the values in Table 12, the fragility curves for CHB30 ORG is developed and presented in Figure 34.

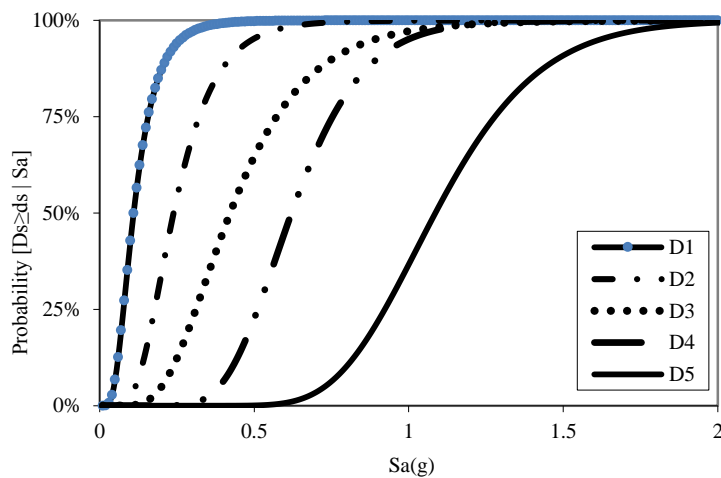


Figure 34: Fragility curves for CHB30 ORG

4.10.3. Fragility curves for YVR14

Using the information in Figure 24, the median and standard deviation (for each damage grade) of the spectral acceleration values at the average maximum period for damage grade 2 (T_{DG2} , Table 10) for YVR14 is calculated and shown in Table 13.

Table 13: Median and standard deviation values of the intensity measures for the damage grades for YVR14

	Median (μ),g	Standard deviation (σ)
DG1	0.30	0.14
DG2	0.53	0.14
DG3	0.86	0.19
DG4	1.33	0.28
DG5	1.44	0.25

Using Equation 6 and the values in Table 12, the fragility curves for YVR14 is developed and presented in Figure 35.

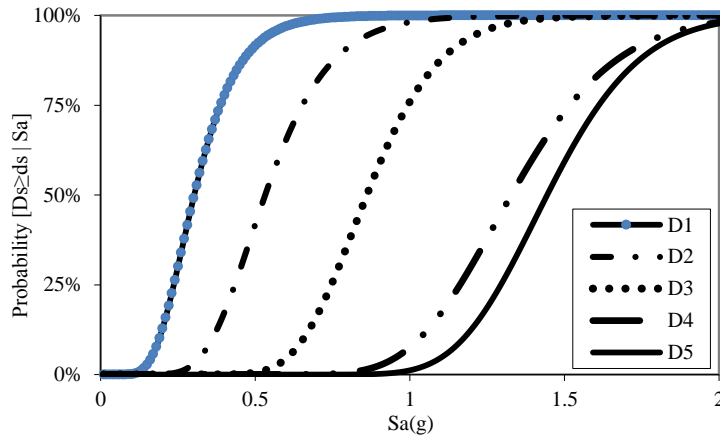


Figure 35: Fragility curves for YVR14

4.10.4. Fragility curves for SECH7

Using the information in Figure 26, the median and standard deviation (for each damage grade) of the spectral acceleration values at the average maximum period for damage grade 2 (T_{DG2} , Table 10) for SECH7 is calculated and shown in Table 14.

Table 14: Median and standard deviation values of the intensity measures for the damage grades for SECH7

	Median (μ),g	Standard deviation (σ)
DG1	0.10	0.04
DG2	0.13	0.08
DG3	0.21	0.07
DG4	0.43	0.11
DG5	0.54	0.13

Using Equation 6 and the values in Table 14, the fragility curves for SECH7 is developed and presented in Figure 36.

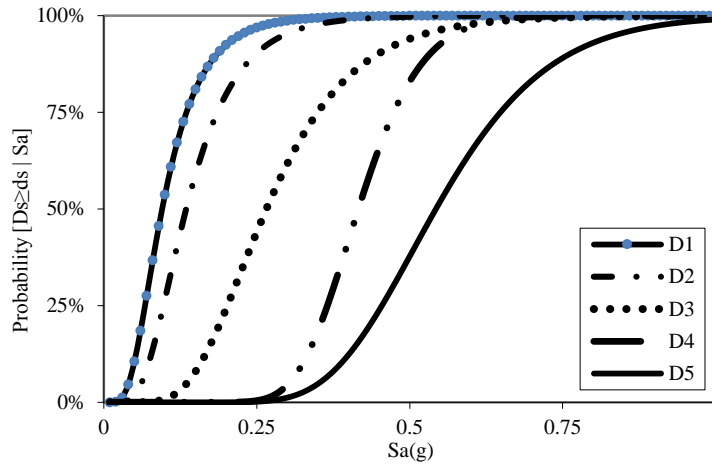


Figure 36: Fragility curves for SECH7

4.10.5. Fragility curves for STD40 ORG

Using the information in Figure 28, the median and standard deviation (for each damage grade) of the spectral acceleration values at the average maximum period for damage grade 2 (T_{DG2} , Table 10) for STD40 ORG is calculated and shown in Table 15.

Table 15: Median and standard deviation values of the intensity measures for the damage grades for STD40 ORG

	Median (μ),g	Standard deviation (σ)
DG1	0.06	0.02
DG2	0.12	0.04
DG3	0.23	0.07
DG4	0.30	0.06
DG5	0.41	0.10

Using Equation 6 and the values in Table 15, the fragility curves for STD40 ORG is developed and presented in Figure 37.

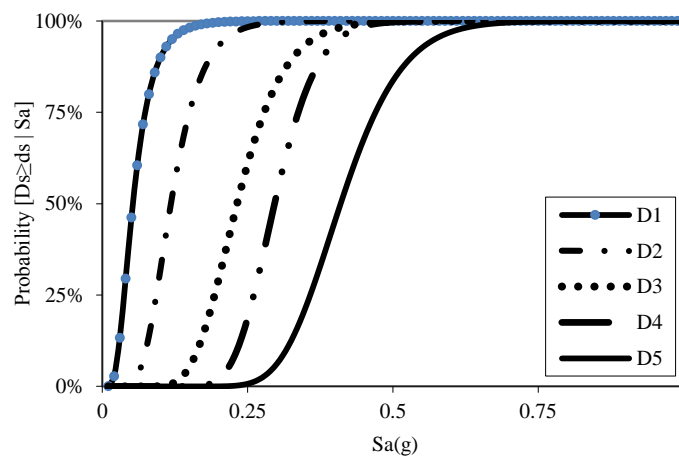


Figure 37: Fragility curves for STD40 ORG

4.10.6. Fragility curves for STD40

Using the information in Figure 30, the median and standard deviation (for each damage grade) of the spectral acceleration values at the average maximum period for damage grade 2 (T_{DG2} , Table 10) for STD40 is calculated and shown in Table 16.

Table 16: Median and standard deviation values of the intensity measures for the damage grades for STD40

	Median (μ),g	Standard deviation (σ)
DG1	0.08	0.03
DG2	0.15	0.06
DG3	0.30	0.07
DG4	0.33	0.09
DG5	0.45	0.17

Using Equation 6 and the values in Table 16, the fragility curves for STD40 is developed and presented in Figure 38.

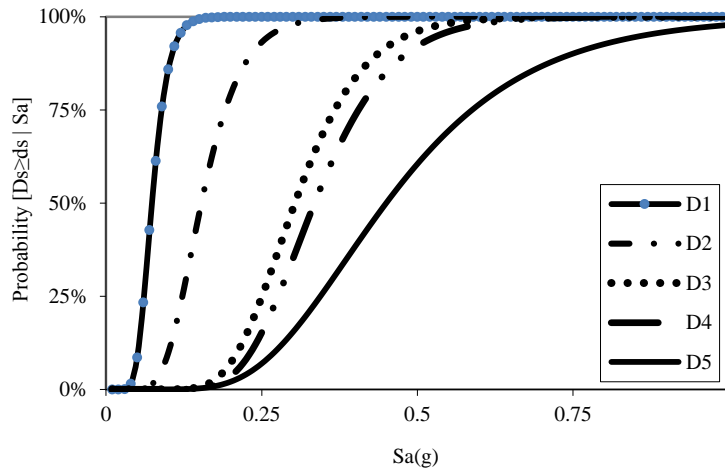


Figure 38: Fragility curves for STD40

4.10.7. Fragility curves for SUVA

Using the information in Figure 32, the median and standard deviation (for each damage grade) of the spectral acceleration values at the average maximum period for damage grade 2 (T_{DG2} , Table 10) for SUVA is calculated and shown in Table 17.

Table 17: Median and standard deviation values of the intensity measures for the damage grades for SUVA

	Median (μ),g	Standard deviation (σ)
DG1	0.06	0.03
DG2	0.10	0.06
DG3	0.21	0.06
DG4	0.35	0.08
DG5	0.46	0.17

Using Equation 6 and the values in Table 17, the fragility curves for SUVA is developed and presented in Figure 39.

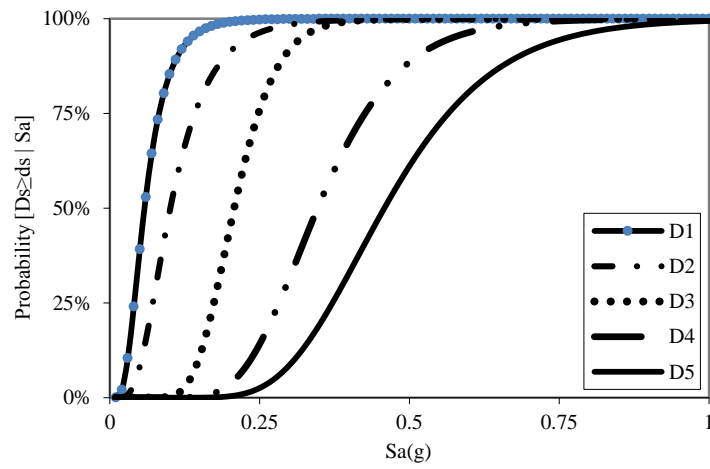


Figure 39: Fragility curves for SUVA

5. Discussion of the results

5.1. Compliance factor of the studied buildings

Compliance factors determine the actual capacity of the building in comparison to its hypothetical capacity was the building evaluated according to pre-standard SIA 2018. Those values are computed for the buildings studied in this report (see Tables 11 and 12). Displacement-based analysis and force-based analysis are used to determine the compliance factors. The main assumptions valid for all the buildings in calculating those values are as follows.

- 1) The material properties for the numerical calculations in this case are considered to be the design values which are smaller than the values presented in Table 3.
- 2) An effective stiffness corresponding to 30% of the stiffness of the un-cracked state is used to consider the stiffness reduction due to cracking.
- 3) For one building (STD40) torsion effects are taken into account according to the simplified approach proposed by Priestley. For the other buildings the torsion effects are neglected because they are negligible (regular buildings Yverdon, Chablais 30) or blocked by the walls in the transverse direction (e.g. SECH7).
- 4) For displacement-based analysis, the storey mechanism occurs at the first floor.
- 5) The values of the corner period of the plateau of the response spectrum (T_c) are used to determine the target displacement according to the EC8 procedure.

Force-based analysis is performed according to the usual procedure proposed in the building codes, more specifically the SIA standards. Storey forces are determined based on the equivalent force method. Behaviour factor is set to $q=1.5$ for unreinforced masonry buildings and to $q=2.0$ for reinforced concrete buildings. The repartition of the storey forces to different walls is performed in pro rata of the stiffness (torsion neglected). Collapse is assumed when the first wall fails. Displacement-based analysis is performed according to the guidelines of SIA D0237 and/or EC8 assumptions.

5.1.1. Building CHB30

The main assumptions in calculating the values of the compliance factors in Table 18 are as follows.

- 1) Torsion effects are neglected.
- 2) The height of the zero moment is constant and corresponds to the storey height i.e. 3.2m.
- 3) Concerning pier height, two different pier heights are considered depending on the location of the walls in the facades (i.e. 2.2m for facades with openings and 3.2m for other facades).
- 4) The storey mass is constant throughout the height, and it is 176 Ton.

Table 18: Compliance factors for CHB30

	$S_a(2.4 \text{ Hz})$	$\alpha_{\text{def,EC8}}^1$	$\alpha_{\text{def,SIA0237}}$	α_{force}^2	T_c
	[m/s ²]	[-]	[-]	[-]	[s]
Zurich SED+ampl.	0.87	4.43	-	0.90	0.40
Zurich Mikro SED	1.15	3.35		0.68	0.40
Zurich SIA BGK A	1.50	2.57		0.52	0.40
Basel SED + ampl.	2.24	1.39	-	0.35	0.60
Basel Mikro SED	3.30	0.90	-	0.24	0.60
Basel SIA BGK C	3.74	0.78	-	0.21	0.60
Sion OT SED + ampl.	2.82	1.07	-	0.28	0.60

Sion OT Mikro Resonance	5.40	0.53	-	0.14	0.60
Sion OT SIA, BGK C	4.60	0.62	-	0.17	0.60
Sion TE SED + ampl.	7.61	0.28	-	0.10	0.80
Sion TE, Mikro. Résonance	4.60	0.49		0.17	0.75
Sion TE, SIA BGK D	5.40	0.41		0.14	0.80

¹ Displacement-based analysis according to EC8 assumptions for strength and displacement capacity,

² Force-based analysis according to Equivalent force method and force distribution according to inertia moment

5.1.2. Building CHB30 ORG

The main assumptions in calculating the values of the compliance factors in Table 19 are as follows.

- 1) Torsion effects are neglected.
- 2) The height of the zero moment is constant and corresponds to the 1.5 storey height i.e. 4.8m.
- 3) The storey mass is constant throughout the height, and it is 134 Ton.
- 4) Equivalent force method, force distribution according to length of the walls.

Table 19: Compliance factors for CHB30 ORG

	$S_a(\text{plateau})$	$\alpha^1_{\text{def,EC8}}$	$\alpha_{\text{def,SIA D0237}}$	α^2_{force}	T_C
	[m/s ²]	[-]	[-]	[-]	[s]
Zurich SED+ampl.	0.87			0.60	0.40
Zurich Mikro SED	1.15			0.45	0.40
Zurich SIA BGK A	1.50			0.35	0.40
Basel SED + ampl.	2.24			0.23	0.60
Basel Mikro SED	3.30			0.16	0.60
Basel SIA BGK C	3.74			0.14	0.60
Sion OT SED + ampl.	2.82			0.19	0.60
Sion OT Mikro Resonance	5.40			0.10	0.60
Sion OT SIA, BGK C	4.60			0.11	0.60
Sion TE SED + ampl.	7.61			0.07	0.80
Sion TE, Mikro. Résonance	4.60			0.11	0.75
Sion TE, SIA BGK D	5.40			0.10	0.80

¹ Displacement-based analysis may not be applied for such buildings with flexible floors,

² Force-based analysis according to Equivalent force method without considering torsion

5.1.3. Building YVR14

For the displacement-based analysis of the building YVR14, two values are determined, one according to the assumption's set of EC8 and the other to the assumption's set of SIA D0237. Assumption's sets include walls strength and ultimate drifts. For EC8, the wall strength is determined with the simplified formulas (shear or rocking) and ultimate drift depends on the failure mode (0.4% in case of shear and 0.8% in case of rocking). For SIA D0237, walls strength is determined according to the stress field theory of SIA 266. The ultimate drift, on the other hand, depends on the normalized compression (0.8% * (1-sigma/fcd)). In addition, SIA D0237 considers a possible sliding collapse in the upper floors, which may reduce the strength of the walls. For the calculations with EC8, this failure mechanism is not

considered. The difference in the obtained compliance factors for YVR14 gives an insight to the uncertainties related to the model assumptions.

The main assumptions in calculating the values of the compliance factors in Table 20 are as follows.

- 1) Torsion effects are neglected.
- 2) The height of the zero moment is constant and it corresponds to the storey height i.e. 2.7m.
- 3) For pier height, a constant value of 2.7m (corresponding to the storey height) is considered.
- 4) The storey mass is constant throughout the height, and it is 300 Ton.

Table 20: Compliance factors for YVR14

	$S_a(3.7 \text{ Hz})$	$\alpha^1_{\text{def,EC8}}$	$\alpha^2_{\text{def,SIAD0237}}$	α^3_{force}	T_C
	[m/s ²]	[-]	[-]	[-]	[s]
Zurich SED+ampl.	0.97	5.56	8.55	1.10	0.40
Zurich Mikro SED	1.35	4.00	6.14	0.77	0.40
Zurich SIA BGK A	1.50	3.60	5.53	0.70	0.40
Basel SED + ampl.	2.63	2.00	2.33	0.40	0.60
Basel Mikro SED	3.35	1.25	1.60	0.31	0.60
Basel SIA BGK C	3.74	1.04	1.37	0.28	0.60
Sion OT SED + ampl.	3.34	1.25	1.61	0.31	0.60
Sion OT Mikro Resonance	5.40	0.60	0.84	0.19	0.60
Sion OT SIA, BGK C	4.60	0.75	1.04	0.23	0.60
Sion TE SED + ampl.	9.01	0.25	0.36	0.12	0.80
Sion TE, Mikro. Résonance	4.60	0.62	0.83	0.23	0.75
Sion TE, SIA BGK D	5.40	0.49	0.67	0.19	0.80

¹ Displacement-based analysis according to EC8 assumptions for strength and displacement capacity

² Displacement-based analysis according to SIA D 0237 assumptions for strength and displacement capacity

³ Force-based analysis according to Equivalent force method and force distribution according to inertia moment

5.1.4. Building SECH7

The main assumptions in calculating the values of the compliance factors in Table 21 are as follows.

- 1) Torsion effects are not considered because they are blocked by the transversal walls.
- 2) The height of the zero moment corresponds to the half of the storey height i.e. 1.4m.
- 3) For pier height, a value of 2.8m (corresponding to the storey height) is considered.
- 4) The storey mass is constant throughout the height, and it is 170 Ton.
- 5) The fundamental period is 2s.

Table 21: Compliance factors for SECH7

	$S_a(0.5 \text{ Hz})$	$\alpha^1_{\text{def,EC8}}$	$\alpha_{\text{def,SIAD0237}}$	α^2_{force}	T_C
	[m/s ²]	[-]	[-]	[-]	[s]
Zurich SED+ampl.	0.2	1.17		1.39	
Zurich Mikro SED					
Zurich SIA BGK A	0.3	0.78		0.92	
Basel SED + ampl.	0.62	0.38		0.45	

Basel Mikro SED					
Basel SIA BGK C	1.12	0.21		0.25	
Sion OT SED + ampl.	0.28	0.83		0.99	
Sion OT Mikro Resonance					
Sion OT SIA, BGK C	1.38	0.17		0.20	
Sion TE SED + ampl.	0.67	0.35		0.41	
Sion TE, Mikro. Résonance					
Sion TE, SIA BGK D	2.16	0.11		0.13	

¹ Displacement-based analysis according to EC8 assumptions for strength and displacement capacity,

² Force-based analysis according to Equivalent force method without considering torsion

5.1.5. Building STD40

The main assumptions in calculating the values of the compliance factors in Table 22 are as follows.

- 1) Torsion effects are considered for displacement-based analysis but neglected for simplification for force-based analysis.
- 2) The height of the zero moment is constant and corresponds to the 1st storey height i.e. 3.57m.
- 3) For pier height, a value of 3.57m (corresponding to the 1st storey height) is considered.
- 4) The storey mass is constant throughout the height, and it is 220 Ton.

Table 22: Compliance factors for STD40 ORG

	$S_a(1.4 \text{ Hz})$	$\alpha_{\text{def,EC8}}^1$	$\alpha_{\text{def,SIA0237}}$	α_{force}^2	T_C
	[m/s ²]	[-]	[-]	[-]	[s]
Zurich SED+ampl.	0.55	1.69		2.13	0.4
Zurich Mikro SED					0.4
Zurich SIA BGK A	0.84	1.18		1.39	0.4
Basel SED + ampl.					0.6
Basel Mikro SED					0.6
Basel SIA BGK C	3.14	0.34		0.37	0.6
Sion OT SED + ampl.	0.78	1.26		1.50	0.6
Sion OT Mikro Resonance	5.40	0.18		0.22	0.8
Sion OT SIA, BGK C	3.86	0.28		0.30	0.6
Sion TE SED + ampl.	1.86	0.77		0.63	0.8
Sion TE, Mikro. Résonance	4.60	0.23		0.25	0.75
Sion TE, SIA BGK D	5.40	0.18		0.22	0.8

¹ Displacement-based analysis according to EC8 assumptions for strength and displacement capacity and considering torsion effects

² Force-based analysis according to Equivalent force method without considering torsion

5.1.6. Building STD40 retrofitted

Compared to the original building, it is assumed that after retrofitting the transversal direction becomes relevant because the torsion effects are restricted by the added RC shear walls. Note that this issue does

not appear in the numerical model. This is due to the different simplifications adopted here for the determination of the compliance factor. Moreover, the frequency related to the displacement-based analysis is significantly higher than the one of the numerical model for the transversal direction (see Table 10). These discrepancies do not facilitate the comparison of the results. The main assumptions in calculating the values of the compliance factors in Table 23 are as follows.

- 1) Torsion effects are neglected (restricted by the added RC shear walls).
- 2) The height of the zero moment is constant and corresponds to the 1st storey height i.e. 3.57m.
- 3) For pier height, a value of 3.57m (corresponding to the 1st storey height) is considered.
- 4) The storey mass is constant throughout the height, and it is 220 Ton.

Table 23: Compliance factors for STD40 after retrofitting

	$S_a(1.67 \text{ Hz})$	$\alpha_{\text{def,EC8}}^1$	$\alpha_{\text{def,SIAD0237}}$	α_{force}^2	T_C
	[m/s ²]	[-]	[-]	[-]	[s]
Zurich SED+ampl.					0.4
Zurich Mikro SED					0.4
Zurich SIA BGK A	1.00	2.35		1.75	0.4
Basel SED + ampl.					0.6
Basel Mikro SED					0.6
Basel SIA BGK C	3.74	0.63		0.47	0.6
Sion OT SED + ampl.					0.6
Sion OT Mikro Resonance	5.40	0.36		0.27	0.8
Sion OT SIA, BGK C	4.60	0.51		0.38	0.6
Sion TE SED + ampl.					0.8
Sion TE, Mikro. Résonance	4.60	0.38		0.28	0.75
Sion TE, SIA BGK D	5.40	0.33		0.24	0.8

¹ Displacement-based analysis according to EC8 assumptions for strength and displacement capacity,

² Force-based analysis according to Equivalent force method without considering torsion

5.1.7. Building SUVA

The main assumptions in calculating the values of the compliance factors in Table 24 are as follows.

- 1) Torsion effects are neglected.
- 2) The total mass is 7010 Ton.

Table 24: Compliance factors for SUVA

	$S_a(1.0 \text{ Hz})$	$\alpha_{\text{def,EC8}}^1$	$\alpha_{\text{def,SIAD0237}}$	α_{force}^2	T_C
	[m/s ²]	[-]	[-]	[-]	[s]
Zurich SED+ampl.	0.45	2.95		0.55	0.4
Zurich Mikro SED					0.4
Zurich SIA BGK A	0.60	2.21		0.41	0.4
Basel SED + ampl.	1.35	0.98		0.18	0.6
Basel Mikro SED					0.6
Basel SIA BGK C	2.24	0.59		0.11	0.6

Sion OT SED + ampl.	0.64	2.07		0.39	0.6
Sion OT Mikro Resonance	3.88	0.34		0.06	0.8
Sion OT SIA, BGK C	2.76	0.48		0.09	0.6
Sion TE SED + ampl.	1.52	0.87		0.16	0.8
Sion TE, Mikro. Résonance	3.69	0.36		0.07	0.75
Sion TE, SIA BGK D	4.32	0.31		0.06	0.8

¹ Displacement-based analysis according to EC8 assumptions for strength and displacement capacity,

² Force-based analysis according to Equivalent force method without considering torsion

In the precedent Tables, SED+ampl. are values based on SED information (hazard curves and amplification functions), Mikro SED are values based on elastic spectra proposed by SED (microzonation studies), Mikro Résonance values are based on design elastic spectra proposed by Résonance (microzonation studies), and SIA BGK are values based on elastic spectra proposed in the building code SIA 261 for the most probable soil class (BGK).

For the buildings YVR14 and CHB30, the results clearly show that force-based analysis leads to compliance factors that are very low in comparison with related deformation-based compliance factors. This is mainly due to the consideration of collapse by the failure of the first wall, and thus neglecting the possible plastic force redistribution in the building. For the other buildings, this issue appears no more because of the very few number of elements considered.

The comparison of the determined compliance factors with the results obtained through the dynamic analyses (see chapter 4) is not always obvious. Due to the different approaches, significant differences may arise in some cases concerning the considered parameters. For building SECH7, the compliance factors are based on a period of 2 s in order to be conservative for the displacement-based analysis but the dynamic analysis is related to a lower period of 1.16 s. For building STD40 before and after retrofitting, the transversal direction remains the critical direction but for dynamic analysis the longitudinal direction becomes the critical one after retrofitting.

It should be noted that target displacements were determined according to EC8 procedures. However, recent research work has shown that such procedures lead to an underestimation of the displacement demands for the period domain corresponding to the plateau of the response spectrum (Michel et al., 2014).

5.2. Comparison with results from other methods

The fragility curves developed in this report for the CHB30 and YVR14 are compared with the curves developed previously in Michel et al. (2009 and 2012) and Oropeza (2011). In the simple analytical method in Oropeza (2011) the capacity curves of the buildings are developed considering the lateral resistance of the individual walls in each direction (push-over analysis). It should be noted that only the weaker direction of the building was used in that work. Using a suitable seismic demand on the building, the spectral displacement value for each damage grade is calculated and a log-normal distribution for the damage grades is then considered to develop the fragility curves. The experimental-based method in Michel et al., on the other hand, considers a non-linear behaviour law based on the experimental modal parameters (resonance frequencies, modal shapes and damping) and a generic non-linear behaviour of those parameters. Damage grades are defined as a function of the inter-story drift from values found in the literature. The methodology ignores local effects in the walls, and does not take into account inelastic effects, so the results are valid only up to DG2 and the curves for DG3 should not be considered. The objective of that simple modelling is to show the importance and limitations of the global elastic building response, based on its modal parameters only, with respect to the local behaviour of the structure.

5.2.1. CHB30 building

Figure 40 presents the fragility curves for the building in Lausanne from three different methods. As seen before, the curves developed in this report used the spectral acceleration values as their engineering demand parameter. For the sake of the comparison here, the spectral displacement values are derived from the linear S_a values. It should be noted that the fragility curves from the simple analytical method is developed for the weaker direction while the nonlinear dynamic analysis method considers both directions.

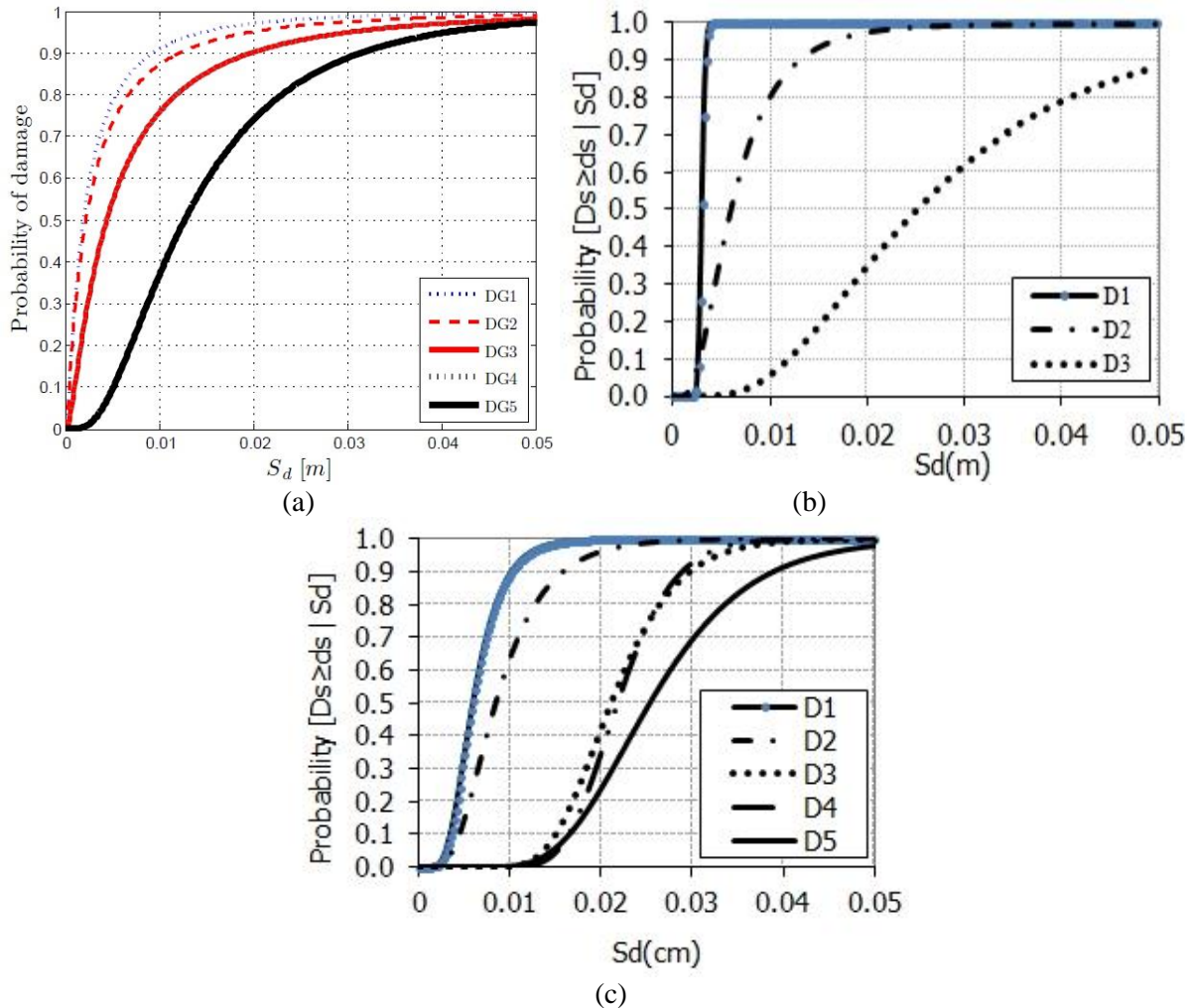


Figure 40: Fragility curves for CHB30 from (a) Oropeza (2011), (b) Michel et al., and (c) nonlinear time-history analysis

To have a better understanding of the damage probability from those curves, the probabilities of exceeding different damage grades are shown in Table 25, given a seismic demand of $S_d=1.5$ cm.

Table 25: Probability of exceeding different damage grade for CHB30 given $S_d=1.5$ cm

	Probability of damage (%)				
	DG1	DG2	DG3	DG4	DG5
Oropeza (2011)	95	92	85	85	60
Michel et al.	100	93	-	-	-
Nonlinear dynamic analysis	98	88	10	5	5

5.2.2. YVR14 building

Figure 41 presents the fragility curves for the building from different sources.

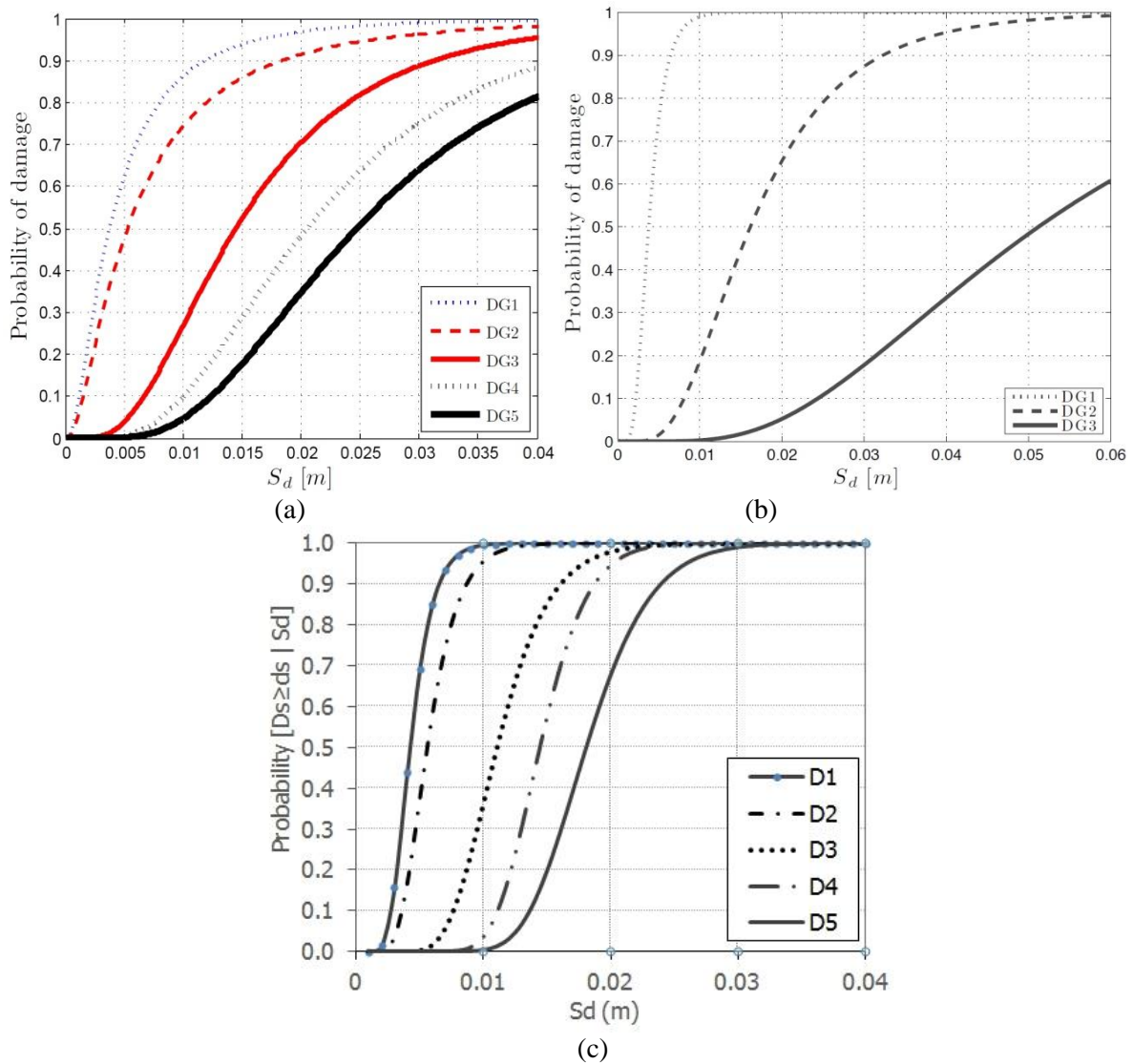


Figure 41: Fragility curves for YVR14 from (a) Oropeza (2011), (b) Michel et al., and (c) nonlinear time-history analysis

To have a better understanding of the damage probability from those curves, the probabilities of exceeding different damage grades are shown in Table 26, given a seismic demand of $S_d=1.5$ cm.

Table 26: Probability of exceeding different damage grade for YVR14 given $S_d=1.5$ cm

	Probability of damage (%)				
	DG1	DG2	DG3	DG4	DG5
Oropeza (2011)	95	85	52	30	18
Michel et al.	100	45	-	-	-
Nonlinear dynamic analysis	100	100	90	60	20

5.2.3. Observations

For CHB30, A comparable trend is seen in the fragility curves from the two sources, Oropeza (2011) and the nonlinear dynamic analysis. For example, the curves for DG3 and DG4 are “completely” and “almost” overlapping from the simple analytical method and the nonlinear dynamic analysis, respectively. However, the curves from Michel et al. show closer results to the dynamic analysis, in general. The premature failure of few interior walls seems to be reason that Oropeza (2011) presents pessimistic curves for CHB30. For that building, the fragility curves from Michel et al. and the nonlinear dynamic analysis have more optimistic values than those from Oropeza (2011).

In term of the fragility curves for YVR14, the results from Oropeza (2011) and the nonlinear dynamic analysis are not comparable directly because of the differences in the periods of the vibration in the two models. Oropeza (2011) considers values of 0.31 sec. and 0.26 sec. as the periods of vibration in the two directions. Those values are 0.22 sec. and 0.2 sec. in the nonlinear dynamic model, performed and presented in this report. As a result, for the same spectral displacement curve, the displacement demands for each model will be different. This results in different median values of S_a for each damage grade. Consequently, the fragility curves will be shifted for the same spectral displacement values. It should be noted that the capacity curves for YVR14 from the two methodologies are similar, despite such differences in the fragility curves.

The fact that the experimental-based curves match the non-linear dynamic analysis for DG1 and in some cases for DG2 shows that the lower damage grades are completely driven by simple parameters such as the fundamental resonance frequency and the max inter-story drift (generic values). For higher damage grades, more local phenomena are involved and deserve more complex models to be reproduced.

5.3. Standard error in the estimation of the engineering demand parameters

The standard errors of estimation (SEE) are used here to determine the preciseness of the calculated engineering demand parameter values (S_a) for each damage grade, based on the number of the number of ground motion records used in the nonlinear dynamic analysis. The SEE values, which is the standard deviation of the measured values divided by \sqrt{n} (n: the number of records for each damage grade), are presented in Table 27.

Table 27: Standard errors of estimation of spectral acceleration values for CHB30

	SEE (% of median)				
	DG1	DG2	DG3	DG4	DG5
CHB30	1.5	4.8	4.1	8.4	10
CHB30 ORG	2.6	3.3	7.2	7.4	9.8
YVR14	3.7	3.1	4.9	9.2	8.0
SECH7	1.3	2.4	2.7	3.9	4.7
STD40 ORG	0.6	1.0	2.0	1.9	3.6
STD40	0.9	2.0	2.4	2.7	6.9
SUVA	0.9	1.9	2.0	2.6	5.6

As seen in Table 27, the standard errors of estimation of the spectral acceleration values in most cases are less than 5% of the estimated median values (less than 10% for all cases).

6. Conclusion

A nonlinear dynamic analysis approach was used to perform the seismic vulnerability evaluation for seven unreinforced masonry and reinforced concrete buildings using the Applied Element Method. 50 ground motions were used in the dynamic analyses, with an overall of 391 time-history 3-D analyses, to determine the distribution of the engineering demand parameter (the spectral acceleration values) at 5 damage grades. Consequently, the lognormal distribution of those measures was used to develop the acceleration-based fragility curves. The method applied in this report is useful for the seismic vulnerability evaluation of buildings in regions for which little observed earthquake damage data is available. The developed fragility curves in this report are used to perform a thorough risk analysis for all the benchmark buildings. Results of that part are presented in a separate report prepared by Risk and Safety AG (Jamali and Kölz 2014).

References

- Applied Science International, 2007. Extreme Loading® for Structures (Version 2.2 B192), Raleigh, NC.
- ATC, 2011. Guidelines for Seismic Performance Assessment of Buildings (75% draft) (Report No. ATC-58). Redwood, CA.
- Belmouden, Y. and P. Lestuzzi. 2007. On The Seismic Vulnerability Assessment of Unreinforced Masonry Existing Buildings in Switzerland. École Polytechnique Fédérale de Lausanne: Lausanne, Switzerland.
- Beyer, K., Tondelli, M., Petry, S., Peloso S., submitted. Dynamic testing of a four storey building with reinforced concrete and unreinforced masonry walls: Prediction and test results, submitted to Bulletin of Earthquake Engineering.
- Bosiljkov V, Page, A., and Bokan-Bosiljkov, V., and Zarnic, R., 2003. Performance based studies on in-plane loaded unreinforced masonry walls, *Masonry International* 16(2):39–50.
- Carol, I., Prat, P. C., and Lopez, C. M., 1997. Normal/Shear Cracking Model: Application to Discrete Crack Analysis, *Journal of Engineering Mechanics* 123(8), 765-773.
- Cattari, S., and Lagomarsino, S., 2008. A strength criterion for the flexural behaviour of spandrels in unreinforced masonry walls. Fourteenth World Conference on Earthquake Engineering. Paper No. 05-04-0041.
- Cervera, M., and Chiumenti, M., 2006. Smearred crack approach: back to the original track, *International Journal for Numerical and Analytical Methods in Geomechanics*, 30(12), 1173-1199.
- D’Ayala, D. and Speranza. E., 2002. An integrated procedure for the assessment of seismic vulnerability of historic buildings, In the Proceeding of the 12th European Conference on Earthquake Engineering. London, UK.
- EC-6. 2005. Eurocode 6: Calcul des ouvrages en maçonnerie-partie 1-1: Règles générales pour ouvrages en maçonnerie armée et non armée. European prestandard (pr EN 1996-1-1 :1995), European Committee for Standardisation.
- Griffith, M. C., Lam, N. T. K., Wilson, J. L., and Doherty, K., 2004. Experimental investigation of unreinforced brick masonry walls in flexure, *Journal of Structural Engineering*, 130(3), 423-432.
- Grünthal. G. 1998 European Macroseismic Scale, EMS-98, Vol. 15. Centre Européen de Géodynamique et de Séismologie, Luxembourg.
- Haldar, A., and Mahadevan, S. 2000. Probability, Reliability and Statistical Methods in Engineering Design. New York: John Wiley & Sons, Inc.
- Ismail, N., Mahmood, H., Derakhshan, H., Clark, W., and Ingham, J. M. (2009). Case Study and Development of Seismic Retrofit Solution for a Heritage URM Building 11th Canadian Masonry Symposium (pp. C5-5). Toronto, Canada.
- Jamali, N., and Kölz, E. 2012. Seismic risk for existing buildings in Switzerland – development of a framework for the probabilistic risk computation, prototype and first application, Risk \rightarrow Safety AG, report prepared for Federal Office for the Environment, 61 p.
- Karbassi, A., 2010. Performanced-based seismic vulnerability evaluation of existing buildings in old sectors of Quebec (PhD thesis), Ecole de technologie supérieure, Montreal. 157 p.

- Karbassi, A., and Nollet, M.J. 2013. Performance-based seismic vulnerability evaluation of masonry buildings using Applied Element Method in a nonlinear dynamic-based analytical procedure, *Earthquake Spectra*, vol. 29, num. 2, pp. 399-426.
- Krawinkler, H., and Miranda, E. 2004. Performance-Based Earthquake Engineering. in Y. Bozorgnia and V. V. Bertero (Eds.), *Earthquake Engineering: From Engineering Seismology to Performance-Based Engineering*: CRC Press.
- Lang, K., 2002. Seismic vulnerability of existing buildings (Ph.D. Thesis), Swiss Federal Institute of Technology, Zurich, Switzerland, 200 p.
- Magenes, G., Calvi, M., 1997. In-plane seismic response of brick masonry walls, *Earthquake Engineering and Structural Dynamics*, 26, 1091–1112.
- Mayorca, P., and Meguro, K., 2003. Modeling Masonry Structures using the Applied Element Method, *Monthly Journal of Institute of Industrial Science, University of Tokyo*, 55(6), 581-584.
- Meguro, K., and Tagel-Din, H. S., 2002. Applied Element Method Used for Large Displacement Structural Analysis, *J Nat Disaster Sci* 24(1), 10.
- Michel C., Guéguen P., Causse M. Seismic vulnerability assessment to slight damage based on experimental modal parameters<<http://dx.doi.org/10.1002/eqe.1119>>, *Earthquake Engineering and Structural Dynamics*, 41(1), 81-98, January 2012.
- Michel C., Lestuzzi P., Lacave C. Simplified non-linear seismic displacement demand prediction for low period structures, *Bulletin of Earthquake Engineering*, Vol 12/4, 2014, pp. 1563-1581.
- Michel C., Oropeza M., Lestuzzi P. Seismic Vulnerability of Existing Masonry Buildings: Final Research Report 2009, Research Report, n°10, EPFL-IMAC, Lausanne, December 2009.
- Milutinovic, Z. V. and Trendafiloski, G. S., 2003. WP4 vulnerability of current buildings, 110 p.
- Okamura H. and Maekawa K., 1991. Nonlinear analysis constitutive models of reinforced concrete, Gihodo Co. Ltd., Tokyo.
- Oropeza, M., 2011. Fragility functions for seismic risk in regions with moderate seismicity, PhD thesis, Ecole Polytechnique Fédérale de Lausanne (EPFL), Lausanne, Switzerland
- Paulay, T., and Priestley, M. J. N., 1992. *Seismic Design of Reinforced Concrete and Masonry Buildings*. John Wiley and Sons, Inc.
- Ristic, D., Yamada, Y., and Iemura, H., 1986, Stress-strain based modeling of hysteretic structures under earthquake induced bending and varying axial loads, Research report No. 86-ST-01, School of Civil Engineering, Kyoto University, Kyoto, Japan
- Sathiparan, N., 2005. Experimental study of retrofit of masonry buildings by PP-band mesh, (M. Eng. Dissertation), University of Tokyo, Japan, 84 p.
- SIA266. 2003. sn 505 266. In Swiss Standards. Swiss Society of Engineers and Architects, Zurich, Switzerland.
- SIA2018. 2004. Vérification de la sécurité parasismique des bâtiments existants, Cahier technique, Swiss Society of Engineers and Architects, Zurich, Switzerland, 2004.

- Tagel-Din, H., and Meguro, K., 2000. Applied Element Method for Dynamic Large Deformation Analysis of Structures, Structural Eng./Earthquake Eng., International Journal of the Japan Society of Civil Engineers (JSCE) 17(2), pp. 215-224.
- Tondelli, M., Petry, S., Beyer, K., 2013. CoMa Walls-Seismic Behaviour of Mixed Reinforced Concrete – Unreinforced Masonry Wall Structures Preliminary Test Report, École Polytechnique Fédérale de Lausanne: Lausanne, Switzerland.
- Tondelli, M., Petry, S., Peloso S., Beyer, K., submitted. Dynamic testing of a four storey building with reinforced concrete and unreinforced masonry walls: Data set, submitted to Bulletin of Earthquake Engineering.
- Vasconcelos, G., 2005. Experimental investigations on the mechanics of stone masonry: Characterization of granites and behavior of ancient masonry shear walls. (Ph.D. Thesis), University of Minho, Portugal, 266 p.

Appendix A. Ground motion records in the nonlinear dynamic analyses

Table A-1: Characteristics of ground motion records used in the nonlinear dynamic analyses

	Record No.	M _s	R (km)	Duration (sec.)	PGA (g)	Soil	Site
European Strong Motion Database	55	6.6	23	15	0.36	Rock	Friuli
	120	5.3	15	13	0.09	Stiff	Friuli
	123	5.3	15	15	0.13	Stiff	Friuli ¹
	126	5.9	21	10	0.45	Stiff	Friuli ¹
	134	5.9	14	22	0.22	Stiff	Friuli ¹
	146	5.9	14	15	0.35	Stiff	Friuli ¹
	171	5.9	18	18	0.15	Stiff	Basso Tirreno
	175	6.2	29	30	0.14	Soft soil	Volvi
	198	7.1	21	18	0.18	Rock	Montenegro
	199	7.1	16	18	0.45	Stiff	Montenegro
	229	6.2	17	15	0.17	Stiff	Montenegro ¹
	242	5.8	5	16	0.15	Rock	Valnerina
	246	5.8	22	16	0.06	Rock	Valnerina
	290	7.1	32	36	0.32	Rock	Campano Lucano
	333	6.7	20	15	0.23	Soft	Alkion
	334	6.7	19	15	0.29	Soft	Alkion
	361	5.4	19	16.5	0.21	Stiff	Umbria
	365	5.9	5	14	0.1	Rock	Lazio Abruzzo
	384	5.3	6	6	0.15	Soft	Lazio Abruzzo ¹
	413	5.8	10	9.5	0.21	Stiff	Kalamata
	419	4.2	1	15	0.33	Stiff	Kalamata ¹
	435	5.8	36	15	0.08	Stiff	Kyllini
	559	5.1	24	18	0.11	Stiff	Pyrgos
	591	5.6	3	14	0.26	Soft	Umbria Marche
	593	5.6	13	15	0.54	Stiff	Umbria Marche
	622	5.3	7	15	0.13	Soft	Umbria Marche ¹
	766	5.4	12	15	0.32	Rock	Umbria Marche ¹
	948	5.4	24	15	0.25	Soft	Sicilia-Orientale
	990	5.3	15	12.6	0.13	Rock	Lazio Abruzzo ¹
	1313	5.9	16	12	0.31	Stiff	Ano Liosia
1715	5.9	14	12	0.33	Stiff	Ano Liosia	
2015	6.2	9	12	0.18	Stiff	Kefallinia ¹	
3802	5.8	7	12	0.47	Rock	Tirana	
5651	5.6	7	4.5	0.38	Very Soft	Benja Luka	
6040	5.4	14	9.9	0.13	Stiff	Kefallinia	
6115	6.6	17	12	0.27	Rock	Kozani	
6131	4.1	12	16	0.28	Soft	Lonian	
Christchurch	CBGS	6.3	10.3	22	0.53	Soft	Botanic Gardens
	CCCC	6.3	7.8	22	0.48	Soft	College
	LPCC	6.3	6.4	22	0.88	Rock	Lyttelton Port
	NNBS	6.3	12	22	0.76	Very Soft	Brighton School
	REHS	6.3	9.4	22	0.72	Soft	Resthaven
	SHLC	6.3	10.3	22	0.31	Soft	Shirley Library
Italian Database	itaca013239	6.3	4.4	15.3	0.49	Stiff	Aquila
	itaca031518	6.0	5.2	8.5	0.32	Stiff	Friuli
	itaca072636	4.6	10	8	0.15	Soft	Umbro-
	itaca094025	6.1	12.1	13.7	0.50	Very Soft	Umria-Marche
	itaca174737	5.4	5	11	0.68	Stiff	Aquila ¹
	itaca183453	6.8	33.3	24.8	0.19	Stiff	Irpinia
itaca210440	4.9	10.6	10	0.19	Stiff	Val Nerina	

¹ Aftershock

Appendix B. Information summary for the benchmark buildings

1. Stone masonry building with RC slabs (Chablais 30 after retrofit, abbreviated hereafter CHB30)

This is a stone masonry building with concrete slabs located in Lausanne. It is a 14m by 12m (in plan) rubble stone masonry with a total number of 6 storeys. The building has 14 walls in the longitudinal direction and 15 walls in the transversal direction. The width of the walls varies between 25 cm to 60 cm, and its average storey height is 3 meters. The thickness of the reinforced concrete slab for this project is assumed to be 20 cm.


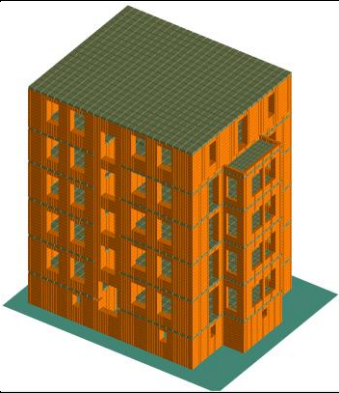
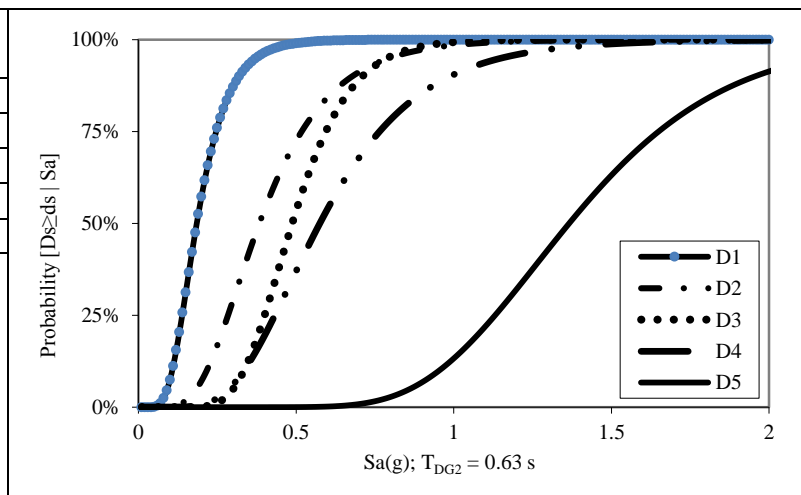
	
Number of stories	6
Year of construction	End of 19 th century
Structural system	Stone masonry
Floor material	RC

Table B-1: Expected properties of masonry units used in the dynamic analyses

Masonry modulus of elasticity (GPa)	1.5
Compression strength (MPa)	10 (\perp bed joints) 4.2 (\perp head joints)
Tensile strength (MPa)	0.75

Table B-2: Median and standard deviation values of the intensity measures for the damage grades for CHB30 + fragility curves

	Median (g)	Standard deviation
DG1	0.19	0.06
DG2	0.36	0.16
DG3	0.49	0.15
DG4	0.58	0.29
DG5	1.37	0.33



2. Stone masonry building with timber slab (Chablais 30 before retrofit, abbreviated hereafter CHB30 ORG)

This building is the same as CHB30, but with timber slabs which represents the original condition of the building before retrofitting took place.


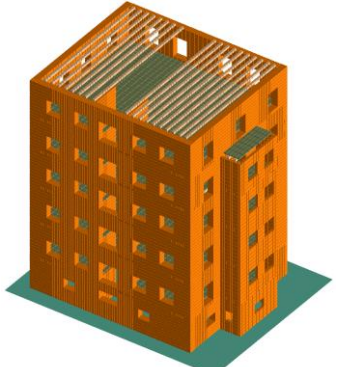
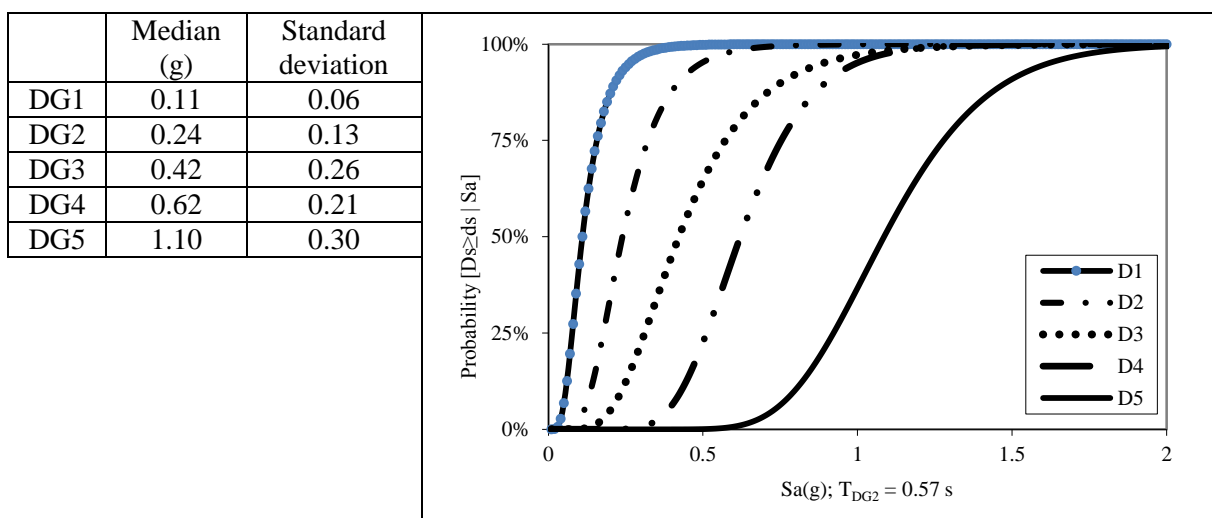
	
Number of stories	6
Year of construction	End of 19 th century
Structural system	Stone masonry
Floor material	Wood

Table B-3: Expected properties of masonry units used in the dynamic analyses

Masonry modulus of elasticity (GPa)	1.5
Compression strength (MPa)	10 (\perp bed joints) 4.2 (\perp head joints)
Tensile strength (MPa)	0.75

Table B-4: Median and standard deviation values of the intensity measures for the damage grades for CHB30 ORG + fragility curves



3. Brick masonry building (*Léon Jaquier 14-16, abbreviated hereafter YVR14*)

This is a brick masonry structure with RC slabs. This 4-storey building is located in Yverdon-Les-Bains. The building is 30 m. by 12 m. (in plan) and it has 37 walls in the longitudinal direction and 16 walls in the transversal direction. The storey height is 2.7 m. The concrete slabs have a thickness of 20 cm.


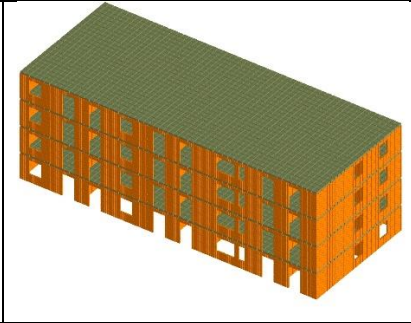
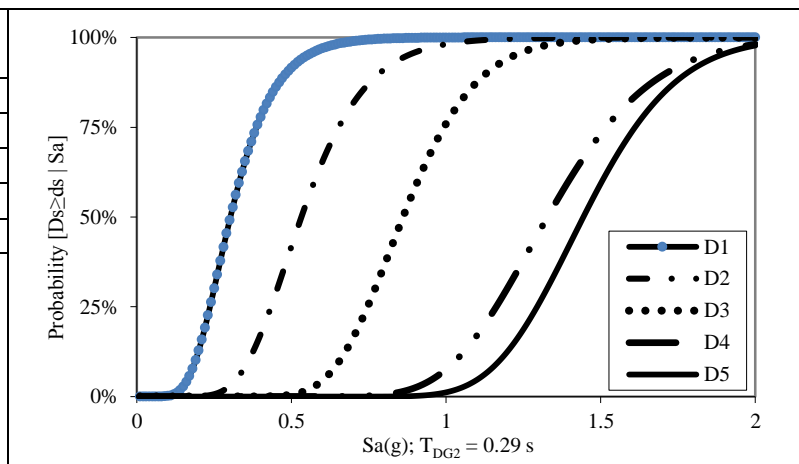
	
Number of stories	4
Year of construction	1955
Structural system	Brick masonry
Floor material	RC

Table B-5: Expected properties of masonry units used in the dynamic analyses

Masonry modulus of elasticity (GPa)	2.0
Compression strength (MPa)	10 (\perp bed joints) 6.3 (\perp head joints)
Tensile strength (MPa)	1.0

Table B-6: Median and standard deviation values of the intensity measures for the damage grades for YVR14 + fragility curves

	Median, (g)	Standard deviation
DG1	0.30	0.14
DG2	0.53	0.14
DG3	0.86	0.19
DG4	1.33	0.28
DG5	1.44	0.25



4. Brick masonry building (Secheron 7, abbreviated hereafter SECH7)

The building is a 7-story brick masonry structure in Geneva with RC slabs (thickness of 18 cm) built in the 60's. The building is 21 m long and 11 m wide with a story height of 2.8 m. The building has several masonry walls in its transvers direction; however, there are a few walls in the longitudinal direction of the building.

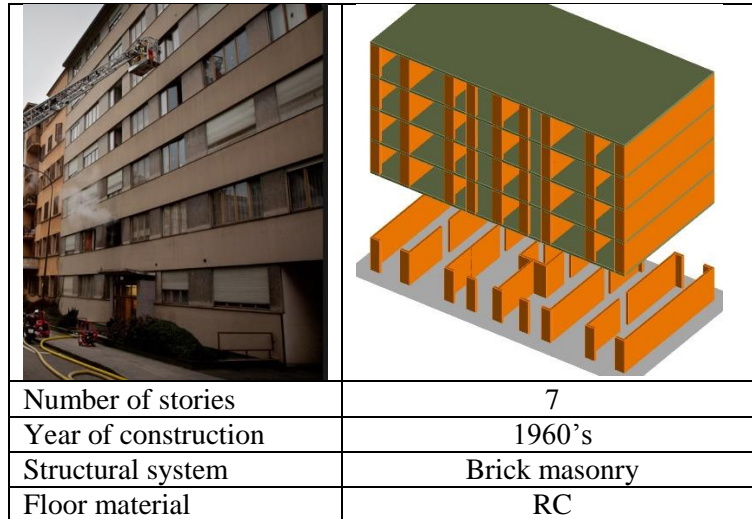
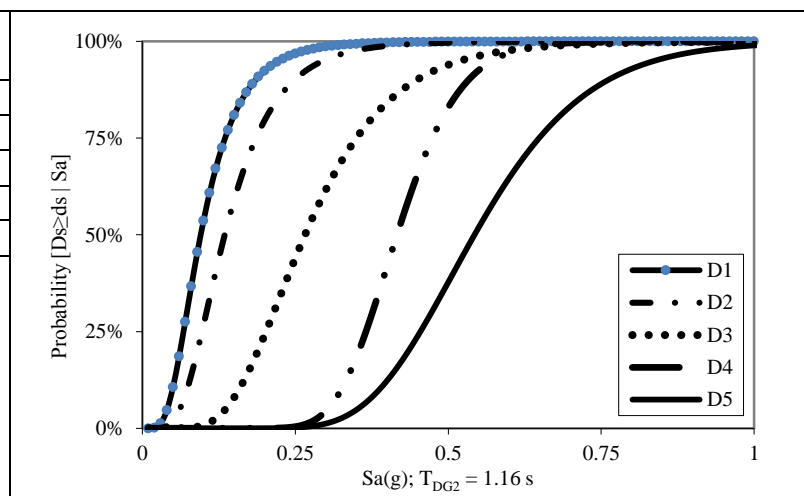


Table B-7: Expected properties of masonry units used in the dynamic analyses

Masonry modulus of elasticity (GPa)	2.0
Compression strength (MPa)	10 (\perp bed joints) 6.3 (\perp head joints)
Tensile strength (MPa)	1.0

Table B-8: Median and standard deviation values of the intensity measures for the damage grades for SECH7 + fragility curves

	Median, (g)	Standard deviation
DG1	0.10	0.04
DG2	0.13	0.08
DG3	0.21	0.07
DG4	0.43	0.11
DG5	0.54	0.13



5. Dual system building: brick masonry/RC (Stand 40, abbreviated hereafter STD40 ORG)

This is a 6-story structure located in Geneva with several masonry walls, two RC shear walls (one of which is very short) and several concrete columns, and RC slabs. The external concrete and masonry walls start from the second floor. This makes the building to have a soft first storey. The building is about 20 m long, 14 m wide and 25 m high.


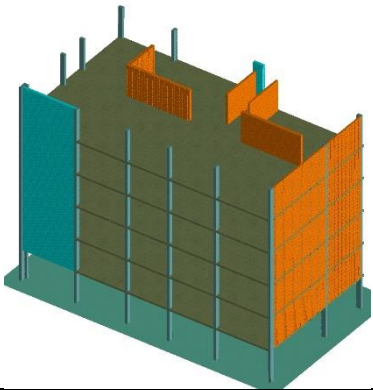
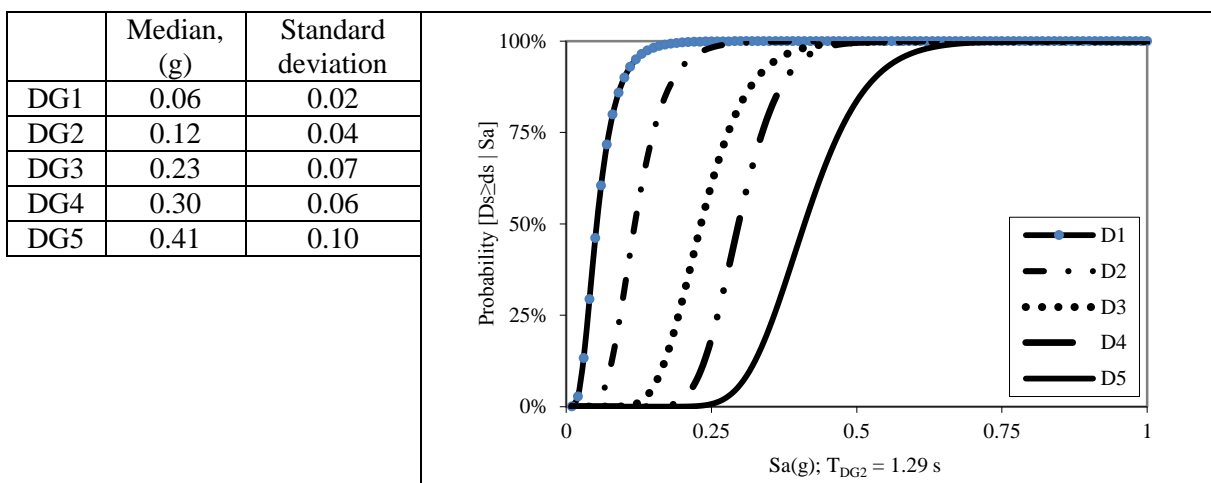
	
Number of stories	6
Year of construction	1956
Structural system	Dual system (URM+RC)
Floor material	RC

Table B-9: Expected properties of masonry units used in the dynamic analyses

Masonry modulus of elasticity (GPa)	2.0
Compression strength (MPa)	10 (\perp bed joints) 6.3 (\perp head joints)
Tensile strength (MPa)	1.0

Table B-10: Median and standard deviation values of the intensity measures for the damage grades for STD40 ORG + fragility curves



6. Retrofitted dual system building: brick masonry/RC (Stand 40, abbreviated hereafter STD40)

This building is the same as STD40 ORG with the external reinforced concrete and masonry walls extended to the first floor to eliminate the soft storey.


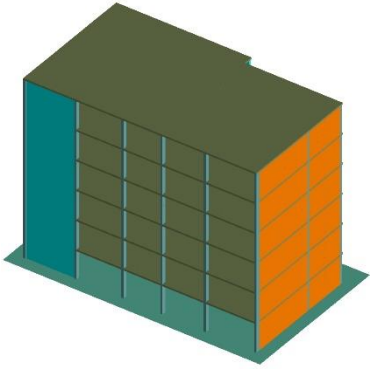
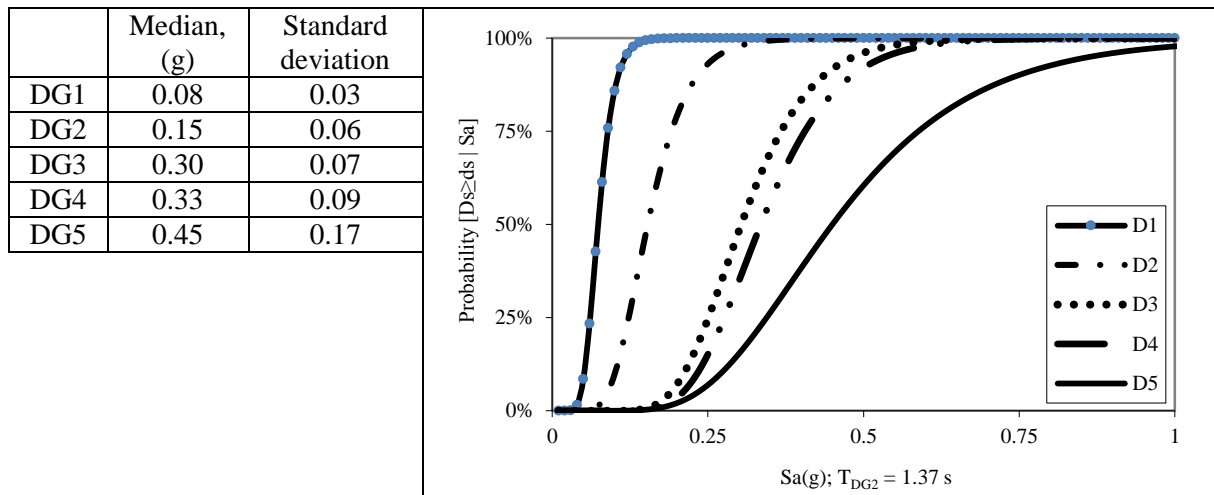
	
Number of stories	6
Year of construction	NA
Structural system	Dual system (URM+RC)
Floor material	RC

Table B-11: Expected properties of masonry units used in the dynamic analyses

Masonry modulus of elasticity (GPa)	2.0
Compression strength (MPa)	10 (\perp bed joints) 6.3 (\perp head joints)
Tensile strength (MPa)	1.0

Table B-12: Median and standard deviation values of the intensity measures for the damage grades for STD40 + fragility curves



7. Reinforced concrete building (Léopold-Robert 23, abbreviated hereafter SUVA)

This is an 11-story RC structure with RC slabs in La Chaux-de-Fonds in Switzerland built in 1967. The building is 33 m long and 15 m wide with a story height of 3 m (4m for the first two floors). The first and the fifth floors are considerably softer than their immediate upper floor.


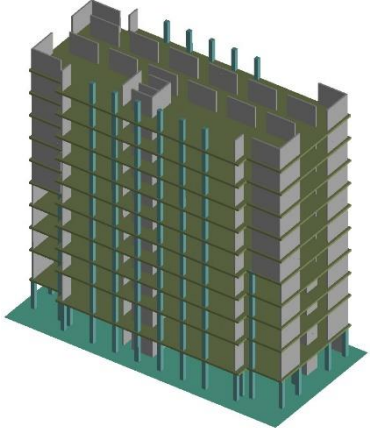
	
Number of stories	11
Year of construction	1967
Structural system	RC
Floor material	RC

Table B-13: Expected properties of masonry units used in the dynamic analyses

Concrete modulus of elasticity (GPa)	22
Compression strength (MPa)	33
Tensile strength (MPa)	3

Table B-14: Median and standard deviation values of the intensity measures for the damage grades for SUVA + fragility curves

